NASA TECHNICAL MEMORANDUM

NASA TM X-52807

NASA TM X-52807

CURRENT NASA RESEARCH IN TURBOJET PROPULSION

Eugene J. Manganiello
Lewis Research Center
Cleveland, Ohio

TECHNICAL PAPER proposed for presentation at Seventh Congress of the International Council of the Aeronautical Sciences, Rome, Italy, September 14-18, 1970

CURRENT NASA RESEARCH IN TURBOJET PROPULSION

Eugene J. Manganiello

Lewis Research Center
Cleveland, Ohio

TECHNICAL PAPER proposed for presentation at

Seventh Congress of the International Council of
the Aeronautical Sciences
Rome, Italy, September 14-18, 1970

NATIONAL AERONAUTICS AND SPACE ADMINISTRATION

CURRENT NASA RESEARCH IN TURBOJET PROPULSION

Eugene J. Manganiello
Lewis Research Center
National Aeronautics and Space Administration
Cleveland, Ohio

E-5685

ABSTRACT

During the past 5 years, the NASA Lewis Research Center has been increasing its effort in turbojet propulsion. Intensive work is now underway in inlet, compressor, combustor, turbine, and nozzle component technology, along with investigations of integrated engine systems, including inlet flow distortion effects on engine stall, and airframe - propulsion system interactions. Recent progress and experimental results are presented in each of these major areas of investigation.

INTRODUCTION

Aircraft propulsion research and development programs underwent a substantial slowdown during the first half of the past decade as a result of the transfer of interest and effort to space activity. This occurred to a greater degree in the U.S.A. than in Europe and was particularly extreme at the NASA (formerly NACA) Lewis Research Center where historical efforts in aircraft powerplant research were redirected almost completely to space propulsion and power generation research.

During the past 5 years, there has been a worldwide resurgence of activity in aeronautics, and significant progress in both civil and military aviation has been accomplished as a result, in no small part, of the advances made in gas turbine propulsion systems. Notwithstanding the present relatively mature state of the art, many research and technology problems remain, and further substantial gains in performance and operational capability lie ahead.

The Lewis Research Center reinstituted activity in aeronautics in 1965 and rapidly rebuilt a substantial effort in advanced airbreathing propulsion systems. A brief outline of this research effort was reported to the Fifth Congress of the ICAS.[1] More detailed results in three specific areas, high-temperature materials,[2] short combustors,[3] and inlets and exhaust nozzles[4] were presented to the Sixth Congress.

The research programs and representative results in the other engine component areas (i.e., compressors and turbines) and on the integrated engine system, including inlet flow distortion effects on engine stall, and airframe - propulsion system interactions are briefly outlined in this present paper. Also, some additional results obtained in the materials, combustor, inlet, and exhaust nozzle research investigations since the Sixth Congress are included in order to provide a reasonably comprehensive, albeit sketchy, picture of the NASA Lewis Research Center current aeronautical research effort. The underlying theme running through the research in the individual component areas is improved engine performance, that is, higher thrust, smaller size and weight, decreased fuel consumption, greater operating stability, etc. Such performance parameters are, of course, important for all types of aircraft and in all flight regimes. They are, however, particularly important for high-performance aircraft at high Mach number and altitude.

Not included herein are many other aircraft propulsion areas under active investigation at Lewis (e.g., V/STOL propulsion, hypersonic propulsion, engine noise reduction, basic research, etc.). They are omitted, not because of their lack of importance, but because of space limitation.

Acknowledgment is made here to the many members of the Lewis Research Center staff who are conducting the described research and who contributed to the preparation of the individual sections of this paper. Most but not all of them are among the authors of the references cited.

MATERIALS

At the Sixth Congress of ICAS, Freche and Hall presented a comprehensive review of the NASA Lewis work in high-temperature alloys.[2] Further progress has been made during the past 2 years and several representative advances are briefly described in the following sections.

Nickel-Tungsten Alloy

Alloying and directional solidification techniques were used to achieve a higher strength material for stator vane use at elevated temperatures than current nickel base alloys. In order to overcome the dropoff in strength above 1900° to 2000° F (1038° to 1094° C) and the relatively depressed melting point of available cast nickel base alloys, a different alloying approach was taken. The nickel-tungsten system, which has a higher melting point than presently used systems, was used as the base, and, in order not to depress excessively the melting point of the final alloy, the number of alloying constituents was reduced compared to currently used nickel-base alloys. The resulting alloy, designated WAZ-20, has a nominal composition in weight percent of 17 to 20 tungsten, 6 to 7 aluminum, 1.4 to 1.6 zirconium, 0.10 to 0.20 carbon, and the balance nickel. It has an incipient melting point (the temperature at which the minor phases melt) of 2375° F (1302° C), which is about 150° F (83° C) higher than that of currently available nickel-base alloys such as IN-100 and B-1900 and is equivalent to that of the strongest cobalt-base alloys.

The 2200° F (1205° C) tensile strength of the alloy is 20 ksi (137.9 MN/m^2). As may be seen in figure 1, this is two to three times higher than that of representative cast, highly-alloyed nickel-base alloys. It is signif-

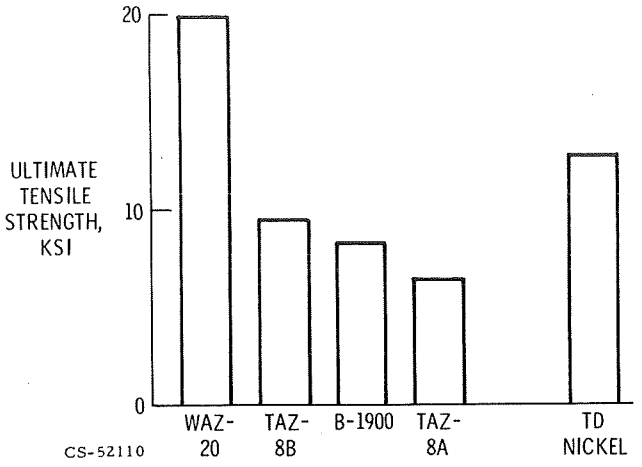

Figure 1. - Strength of nickel-base alloys at 2200° F.

icant that WAZ-20 is also stronger at this temperature than TD nickel, a dispersion-strengthened nickel-base material which exhibits a strength advantage over conventional, highly alloyed cast nickel-base materials above 2000° F (1094° C).

The application of directional solidification techniques in which the grain structure is alined parallel to the major stress axis resulted in improved tensile strength, generally increased ductility, and increased stress rupture life compared to the random polycrystalline form of the alloy. Figure 2 illustrates the twofold increase in 15 ksi (103 MN/m^2) rupture life and the approximately 50° F (28° C) increase in use temperature obtained by directional solidification with WAZ-20.

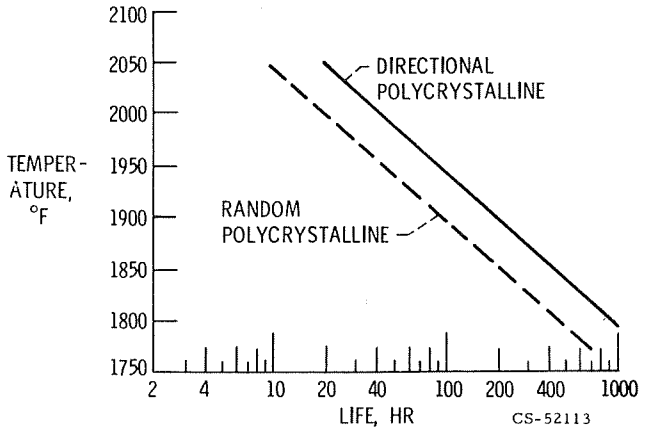

Figure 2. - Effect of directional solidification on rupture properties of WAZ-20. Stress, 15 ksi.

Exposure of WAZ-20 to intermediate temperatures for 1000 hours did not result in the formation of any embrittling phases, a potentially serious problem for long-time engine applications. In fact, the alloy's impact strength after such exposure was 4 to 10 times higher than that of currently available cast nickel- and cobalt-base alloys.

The combination of properties, 150° F (83° C) higher incipient point, substantially greater strength at 2200° F (1205° C), microstructural stability, substantially higher impact strength, and the alloy's amenability to directional solidification, suggest that it has considerable potential for application to the stator vanes of advanced turbine engines. More detailed information on this WAZ-20 alloy is contained in reference 5.

Prealloyed Powder Metals

Inasmuch as most high-strength, nickel-base alloys are highly alloyed, severe macrosegregation and microsegregation can occur in castings so that their full strength potential is frequently not realized. Furthermore, segregation increases the difficulty of forming alloys from the ingot starting stock.

The use of prealloyed powders affords a means of overcoming the problems inherent in conventional casting and hot-working operations of superalloys. By atomizing the molten alloy with an inert gas jet, each metal droplet is subjected to rapid solidification rates, and this contributes to a more homogeneous structure upon subsequent compaction of the powder. Use of inert gas in the atomization process reduces the oxygen content of the powders, which, in turn, militates against the formation of large oxide particle inclusions and facilitates powder compaction by preventing the formation of tightly adherent oxide films on the powder particles.

The prealloyed powder approach is under intensive investigation with a number of experimental and commercially available nickel-base alloys. This approach has been applied successfully to the NASA TAZ-8A alloy and the commercial alloy 713C, as reported in reference 6. The significant increases in intermediate temperature tensile strength over the cast counterparts of these alloys achieved with the prealloyed powder products is illustrated in figure 3 for TAZ-8A. Room-temperature ultimate strength was almost doubled from 128 ksi (882 MN/m^2) to 228 ksi (1570 MN/m^2). This increase is due to the finer grain size of the powder product compared to the cast alloy and possibly to some retained work in the as-extruded powder product. A crossover in the tensile strength curves occurs somewhat above 1400° F (760° C) because at higher temperatures the finer grain size of the powder product is

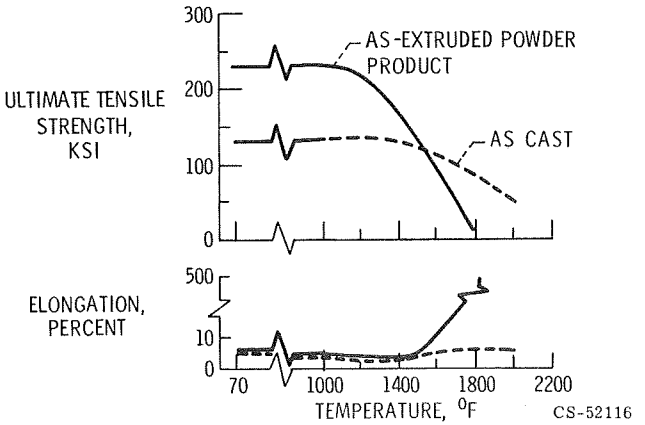

Figure 3. - Improvements in tensile properties of TAZ-8A.

detrimental to strength. At these high temperatures another aspect of as-extruded prealloyed powder behavior becomes evident; namely, superplasticity as indicated by the elongation curve of figure 3. This is further illustrated in figure 4, which compared a test bar before and after test at 1900° F (1038° C). The more than 600 percent neck-free elongation observed in the test specimen is indicative of micrograin superplasticity.

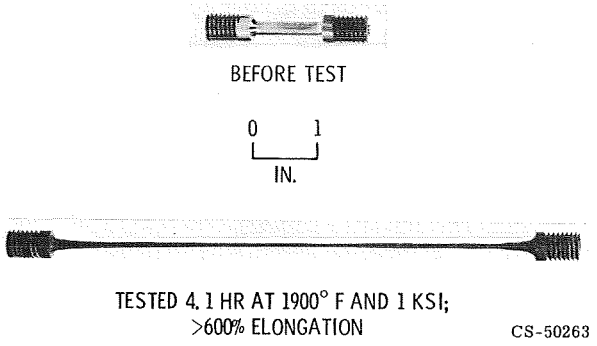

Figure 4. - Superplasticity in as-extruded TAZ-8A powder product.

The superplasticity phenomenon has been utilized to deform the prealloyed powder product into desired shapes by simple hot pressing. This formability is illustrated in figure 5, which shows a small turbine blade of TAZ-8A prealloyed powder product. It was hot pressed to shape at 2000° F (1094° C), a temperature at which the powder product is superplastic, between the two halves of the cast TAZ-8A dies shown in the lower part of the figure.

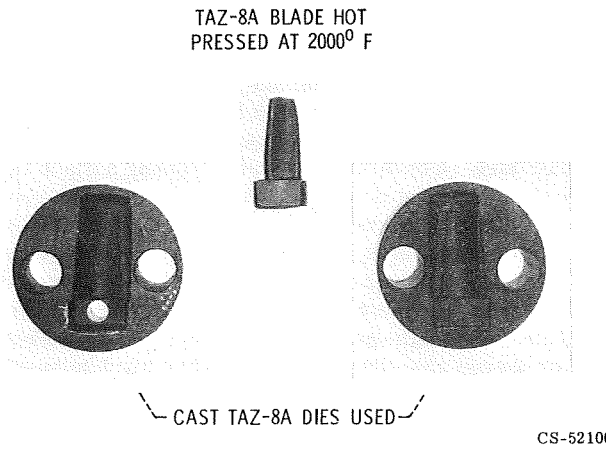

Figure 5. - Formability of TAZ-8A prealloyed powder product.

The superiority of the prealloyed powder process may possibly be extended beyond the intermediate temperature range if superplasticity can be eliminated and the alloy's resistance to deformation restored once it has been formed into a desired shape. Application of high pressure and temperature above the incipient melting point suggests a means of achieving the coarseness of microstructure and the solidification structure, both of which may be needed to improve high-temperature strength of prealloyed powder products.

Metal Fiber Composites

Fiber composite materials have been the subject of intensive research in recent years because they offer the potential to provide materials with improved strength and rigidity. For example, the strength and rigidity of boron fibers can be combined with the ductility and toughness of aluminum. Similarly, the strength of refractory metal fibers at high temperatures can be combined with the superior oxidation resistance and ductility of superalloy matrix materials.

After early investigations with model systems, such as tungsten fibers in copper, indicated that the strength of fibers can be realized in composites, a program was conducted to combine tungsten alloy fibers in a superalloy matrix.[7,8] The goal was to achieve a composite for longtime, high-temperature applications such as turbojet engine turbine buckets. Initially serious problems were encountered in effectively bonding fibers to the matrix while controlling matrix-fiber reaction. Subsequently, matrix-fiber reactions were successfully controlled and composites fabricated with the strengths shown in figure 6.

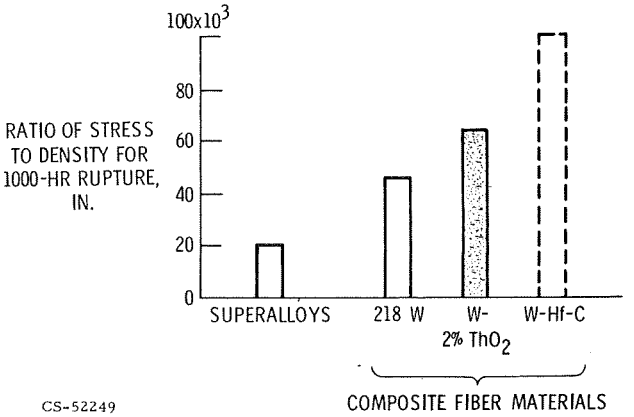

Figure 6. - Stress-rupture strength of superalloy composites. Fiber content, 70 volume percent; temperature, 2000° F.

Bar graphs of ratio of stress to density for rupture in 1000 hours at 2000° F (1094° C) are plotted for three composites, and for conventional superalloys (fig. 6). The first composite, with 70 volume percent 218 tungsten (W) alloy wire, is over twice as strong as the superalloys. The W-2ThO_2 composite strength is 40 percent stronger than the 218 W composite and three times that of the superalloys.

The bar graph with the dashed lines represents the strength expected to be achieved for composites reinforced with tungsten-hafnium-carbon (W-Hf-C) wire. This alloy, developed at Lewis, is one of the strongest available. Wire drawing procedures are currently being developed for this alloy, and a limited quantity of wire has been produced. The strength plotted for the W-Hf-C wire composite represents a calculation of the composite strength based on the wire strength results obtained to date. For the calculation, it was assumed that 80 percent of the wire strength was retained in the composite. That retention value is similar to those achieved for the other two composites. The strength value of the W-Hf-C composite is five times that of the superalloys. Whereas

the ratio of rupture strength to density achieved with the W-2ThO_2 fiber composite represents a potential increase of 200° F (111° C) in turbojet engine turbine blade use temperature, the W-Hf-C composite should indicate the potential for a further significant increase in operating temperature.

FANS AND COMPRESSORS

The general trend in fan and compressor technology is toward higher stage pressure ratios, greater blade tip speeds, and lighter weight; all of which must be achieved with little or no loss in efficiency. Furthermore, fans and compressors are required to operate efficiently over a wide range of flight conditions while maintaining an adequate stall margin in the environment of engine transients, inlet flow distortions, and deteriorations in component performance due to wear, dust accumulations, or foreign object damage. The final compromise between lightweight, high component efficiency, and stall margin is, of course, dependent on the requirements of the particular application.

Stage Pressure Ratio

An increase in stage pressure ratio can be achieved by increasing either the rotor blade tip speed, the aerodynamic blade loading, or a combination of both. The present NASA fan and compressor research program covers a range of both rotor blade tip speeds and aerodynamic loadings as illustrated in the lower portion of figure 7. Blade tip speeds to at least 1800 feet per second (548 m/sec) are being studied. The symbols indicate a number of advanced transonic fan or compressor

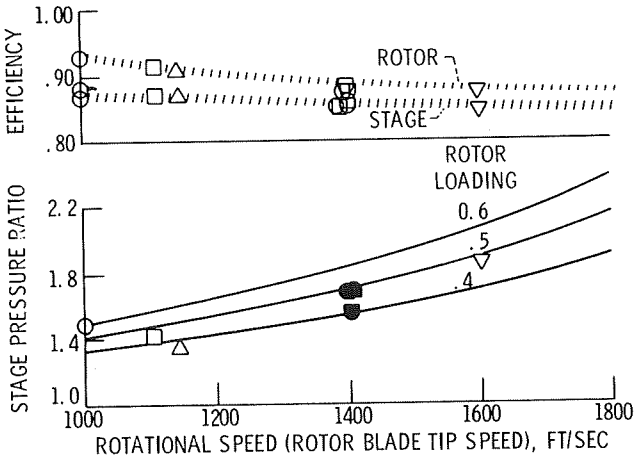

Figure 7. - Fan and compressor stage performance trends.

stages (open symbols) or rotors (solid symbols) that have been tested to date. The stage pressure ratios range from 1.5 at a blade tip speed of 1000 feet per second (300 m/sec) to 1.85 at 1600 feet per second (490 m/sec). With one exception, the rotor aerodynamic loadings (Lieblein diffusion factor) all exceed a value of 0.4 and thus are significantly greater than those normally employed in conventional practice. (The diffusion factor is a measure of velocity deceleration over the blade suction surface.) To maintain high levels of efficiency at the relatively high blade loadings and rotational speeds shown, it is imperative that excessive increases in flow losses be avoided. Consequently, the blading for these advanced stages was specifically selected to achieve low flow losses, and thus relatively high efficiencies. For the most part, multiple circular arc blade sections are used for advanced compressor stages. The camber line for a multiple circular arc blade consists of two circular arcs of different radii that are mutually tangent at the point of juncture. The pressure and suction surfaces of the forward and rearward portions of the blade are also composed of circular arcs. At very high blade tip speeds, it appears desirable to employ the concept of precompression for the supersonic portion of the multiple circular arc blade to minimize losses associated with the stronger shock patterns at increased speeds.

In the upper portion of figure 7, both the measured rotor efficiency (upper shaded line) and the stage efficiency (lower shaded line) are presented. The difference between rotor and stage efficiency is due to flow losses in the stator blade rows. At the lower blade tip speed of 1000 feet per second (300 m/sec), a high rotor efficiency of 0.93 was obtained, whereas the 1600 foot-per-second (490-m/sec) tip-speed rotor had a maximum rotor efficiency of about 0.87. The corresponding stage efficiencies were 0.865 and 0.845. Thus, although rotor efficiencies tend to decrease somewhat with increasing blade tip speed the lower curves indicate that it is possible to maintain good overall stage efficiencies for fans and compressors over a wide range of blade tip speeds - and at higher stage pressure ratios than are generally used in current engines.

As shown in figure 7, the greater difference between rotor and stator efficiency occurs at the lower blade tip speeds. In order to obtain high pressure ratios at relatively low blade tip speeds, the stator must operate at high flow Mach numbers and at high levels of aerodynamic loading. Both these factors contribute to greater stator loss. Conversely, the stage having a blade tip speed of 1600 feet per second (490 m/sec) shows relatively lower stator loss because of more conservative values of stator inlet Mach number and blade loading encountered. Although a high-speed design can have relatively low stator losses, lower rotor efficiencies are obtained with high-speed rotors because of the increased rotor losses associated with the higher Mach numbers encountered. Hence, for high-pressure-ratio stages, decreased stator losses for low-speed designs and improved rotor efficiency at high blade tip speeds are two areas in which NASA is conducting further studies.

A major portion of the high stator loss observed for high-pressure-ratio - low-speed stages results from flow separation that occurs in the corners formed by the stator blades and the annulus walls. Several schemes such as blowing, bleeding, and boundary layer control are being considered to minimize these "end-wall effects." One such method is illustrated in figure 8. Suction is applied by means of a narrow slit along the blade suction surface (at the inner wall only) to alleviate or reduce the flow separation that occurs in this region and thereby reduce the end losses and delay blade stall. The effectiveness of slit suction for the 1000 foot-per-second (300-m/sec) fan stage is illustrated by the two loss curves shown. The solid curve represents the no-

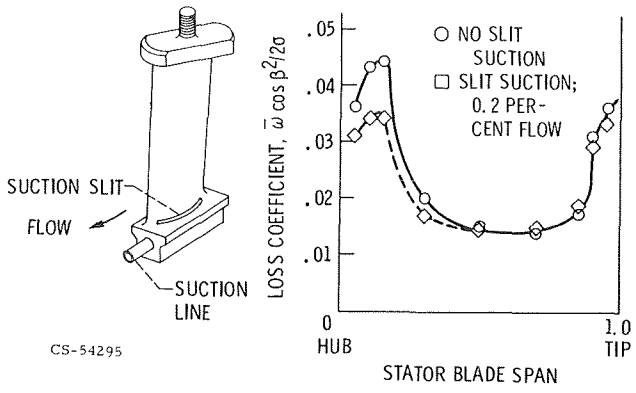

Figure 8. - Effect of slit suction on stator losses.

suction case, whereas the dashed line represents operation with a slit suction flow of 0.2 percent of the total through-flow of the stage. Losses in the hub region were reduced as much as 20 percent, and some improvement is noted out to the midspan of the blade. For this particular fan stage[9] the application of stator hub slit suction improved overall stage efficiency about $1\frac{1}{2}$ points from 0.865 to 0.880 (tailed data point of fig. 7). Some increase in stall margin was also noted.

Stall Margin

In addition to good efficiency, a useful high-pressure-ratio transonic stage requires an adequate flow range, or stall margin. The rotor for the 1600 foot-per-second (490-m/sec) stage is shown in figure 9, and the performance map for the stage is presented in figure 10. At design speed, the peak efficiency of 0.845 occurs at a pressure ratio of 1.85 as previously noted.

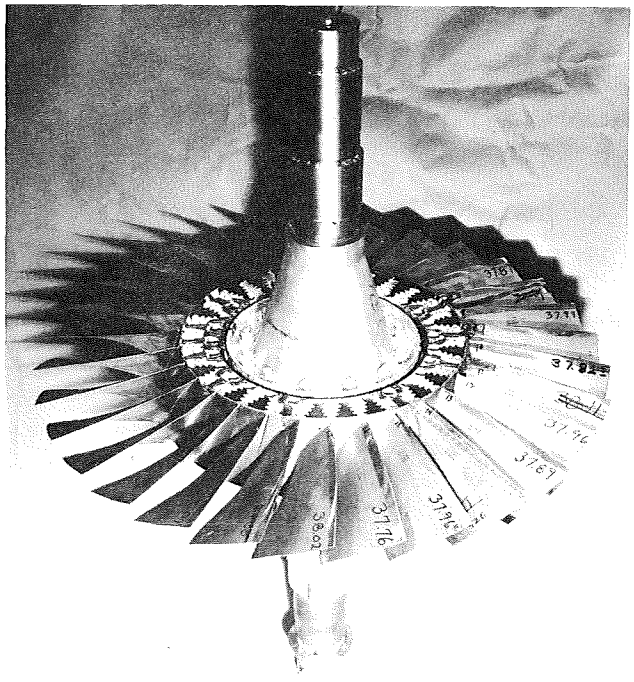

Figure 9. - Highly loaded transonic compressor rotor. Blade tip speed, 1600 feet per second.

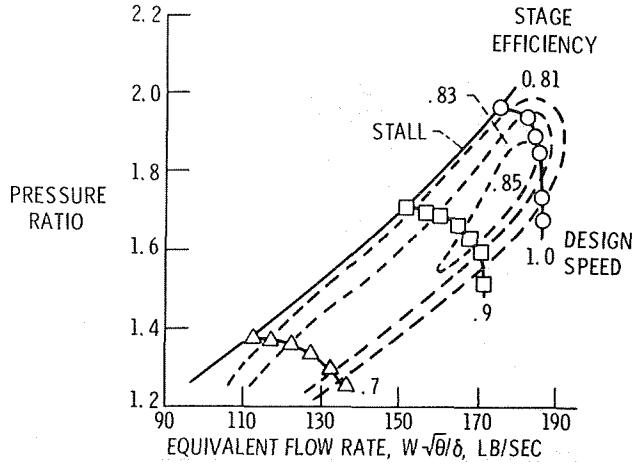

Figure 10. - Transonic fan stage performance.

A substantial range in both pressure ratio and weight flow between the point of maximum efficiency and stall is indicated. This constitutes a stall margin of about 18 percent, which is comparable to that obtained for stages operating at considerably lower tip speeds. Thus, this stage, which demonstrates good efficiency at a high pressure ratio and with adequate stall margin as well, is suitable for a relatively wide range of fan applications. Design details for the 1600 foot-per-second (490-m/sec) stage are reported in reference 10.

Maintaining good efficiency and stall margin at both subsonic and supersonic cruise conditions requires some degree of stage rematching. One approach to stage rematching that has been investigated is the variable blade camber concept[11] shown in figure 11. For takeoff and

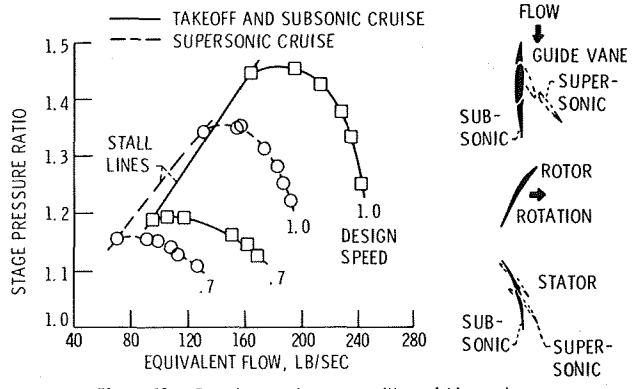

Figure 11. - Fan stage performance with variable camber vanes.

subsonic cruise conditions, the inlet guide vanes and the first-stage stator blades were cambered as shown by the shaded blade sections of figure 11 and the photograph of figure 12(a). These camber settings provided the proper inlet relative flow angles to the first- and second-stage rotors. As indicated by the performance map, the stall margin for takeoff and subsonic cruise was adequate. The stage pressure ratio was about 1.45 and the stage efficiency (not shown) was 0.90. At supersonic cruise in the Mach 2.0 regime, the equivalent speed has now been reduced to about 0.7 and the compressor oper-

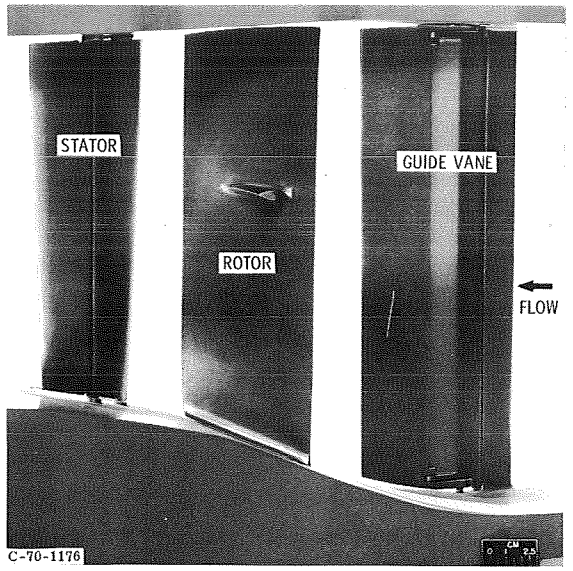

(A) TAKEOFF AND SUBSONIC CRUISE CONFIGURATION.

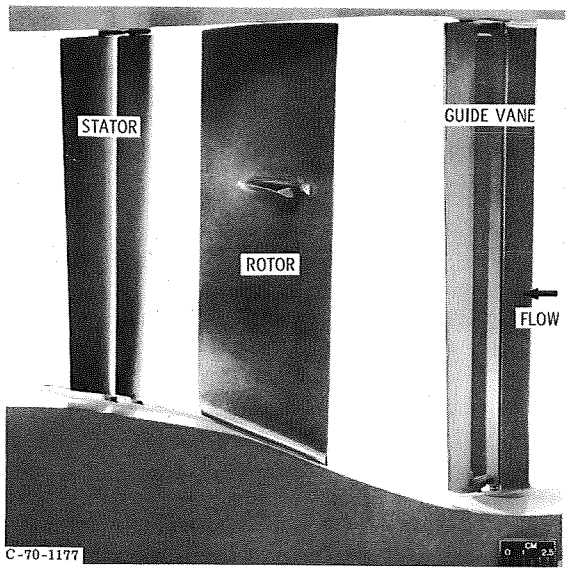

(B) SUPERSONIC CRUISE CONFIGURATION.

Figure 12. - Variable geometry guide vane and stator.

ating line (without rematching) would likely be at or near the stall line, where a relatively low efficiency can be expected. To increase stall margin and efficiency at this supersonic flight condition, the inlet guide vanes are recambered (as shown by the dashed sections of fig. 11 and the photographs of fig. 12(b)) to again provide, insofar as possible, the proper flow conditions to the first-stage rotor. Similarly, the stators must be recambered to improve flow conditions to the succeeding rotor. The performance obtained with the vanes reset to the supersonic cruise configuration is shown by the dashed lines. The pressure ratio produced at 0.7 equivalent speed (for flight Mach numbers above 2.0) is slightly lower for the supersonic cruise setting; however, the stall line was extended to lower weight flows compared to those for the subsonic cruise setting. Under these conditions the stage operated with good stall margin and at an efficiency comparable to that obtained for the subsonic cruise configuration at design speed. The data of figure 11 are for a single stage design. However, other studies indicate that the application of the variable blade camber concept to multistage compressors will likely result in even greater improvements than those noted in figure 11, particularly with regard to stall margin. Thus, blade recambering can provide stage matching required for efficient operation at both subsonic and supersonic flight conditions.

Airflow Distortion

The problem of inlet airflow distortion and its effect on compressor performance is another area of research receiving considerable attention at present.

At present there is no available method that adequately relates compressor performance with the type or degree of airflow distortion. And before such a method can be developed, it first appears necessary to have a good understanding of the basic mechanisms involved. This requires detailed measurements of flow conditions at both the inlet and the discharge of the rotor.

Some examples of circumferential variations of various measured parameters are presented in figure 13. The data are for a rotor having a 1375 foot-per-second (420-m/sec) blade tip speed and operated at a near-stall condition with circumferential distortion that was produced by a screen covering a 90° arc of the inlet annulus. The decrement in inlet total pressure was about

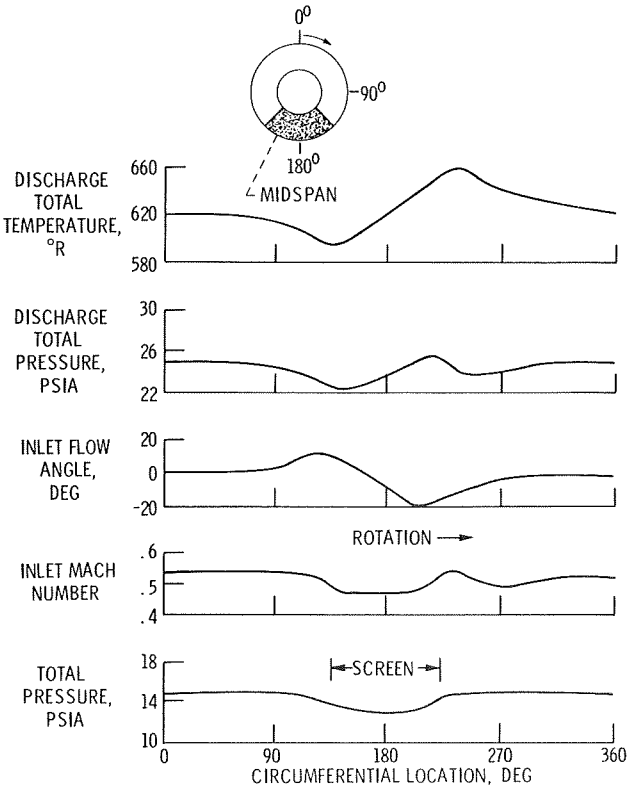

Figure 13. - Circumferential variation in measured flow parameters. Midspan data: near stall; 100-percent design speed; blade tip speed, 1375 feet per second.

10 percent with correspondingly reduced Mach numbers in the distortion region as shown. Interestingly, the combined effect of the screen and the pumping action of the rotor results in unsymmetrical flow conditions at the rotor inlet, as evidenced by the wide variations in the measured inlet flow angles shown. As the rotor blade enters the distorted region, the flow turns increasingly more in the direction of rotor rotation, which reduces the aerodynamic loading of the blade. However, as the blade travels through the distorted region, the inlet flow angles change more and more in the direction opposite to rotation until, upon leaving the distorted region, the blade is operating at loadings which are far in excess of those that would normally cause stall under steady-state conditions. These changes in loading are clearly evidenced by the wide circumferential variations in measured rotor discharge total temperatures and pressures (upper part of fig. 13). Data comparisons show that the maximum discharge temperature (or temperature rise) shown is significantly greater than the corresponding temperature measured with uniform inlet flow under similar operating conditions. However, these unusually high discharge temperatures (or blade loadings) existed over a relatively small portion of the circumference, 90° or less. For the remaining portion of each blade revolution, the discharge temperatures and blade loadings were all less than those experienced with uniform flow. This loading of the blades over the major portion of the annulus partly accounts for the loss in overall pressure ratio experienced with circumferential inlet airflow distortion. Also, the fact that the blade experiences the unusually high blade loadings for only short periods of time may explain the ability of the blade to operate, with no apparent stall, at loadings which are greater than those indicated for uniform flow.

The data of figure 13 are typical of the type of distortion data being obtained in order to provide a better understanding of the basic mechanisms involved with inlet flow distortion and its relation to the performance of fans and compressors.[12,13] The present NASA program on inlet flow distortion includes studies such as (1) effects of tip and hub radial distortion, as well as circumferential distortion, (2) effects of distortion levels and extents, (3) effects on both single and multistage fans and compressors, and (4) effects of both steady-state distortion (screens) and time-unsteady distortions (dynamic) on full-scale jet and fan-jet engines.

COMBUSTORS

Since the 1968 report[3] on combustors, additional work has been done with the segments of short annular combustors; full-annulus combustors have been tested, and further improvements in performance have been obtained. As an example of this work, the current status of one of the short combustors, the twin-annulus ram-induction combustor, is discussed. Figure 14 shows a photograph of the combustor liner. This view shows the fuel nozzle positions (32 in each annulus) and the scoops that are used to admit the primary and secondary air into the combustor. Each scoop has turning vanes to turn the high-velocity air into the combustor. The airflow is at a high velocity with only a minimum of diffusion ahead of the combustor. The high velocity of the

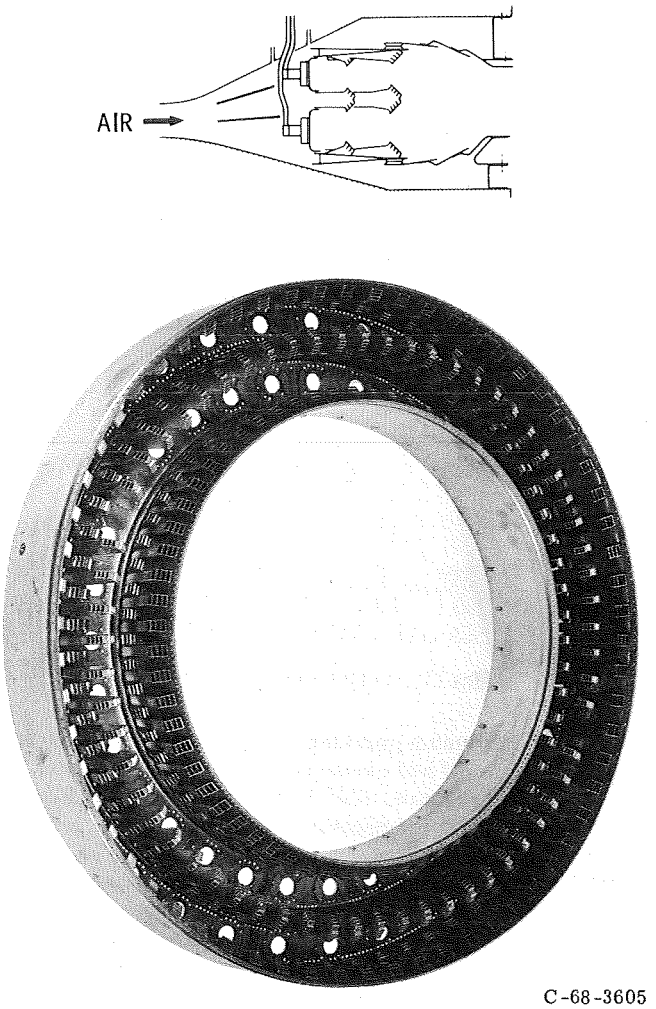

C-68-3605

Figure 14. - Twin-annulus ram-induction combustor liner.

air, the steep injection angle, and the large number of air admission scoops serve to promote rapid mixing of air and fuel in the primary zone and of diluent air and hot gases in the mixing zone. This design results in a short overall combustor length and improved exit temperature profiles. The center shroud scoops divide the combustor into two concentric annuli, each with a higher ratio of length to height than would be available in a single-annulus combustor of the same overall length.

This combustor has an outer diameter of 41.8 inches (106.4 cm), an inner diameter of 21.4 inches (54.4 cm), and an overall length from compressor exit to turbine inlet of 20.25 inches (51.4 cm). It was designed for a turbofan engine to cruise at a Mach number of 3 at an altitude of 65 000 feet (19 800 m) with a core airflow of 280 pounds per second (127 kg/sec) at takeoff.

The lengths of various combustors from existing aircraft turbine engines are compared in figure 15. Separate curves are shown for each of the basic combustor types: can, can-annulus, and annular. The twin-annulus combustor is approximately one-third shorter than single-annulus combustors designed for the same airflow rate.

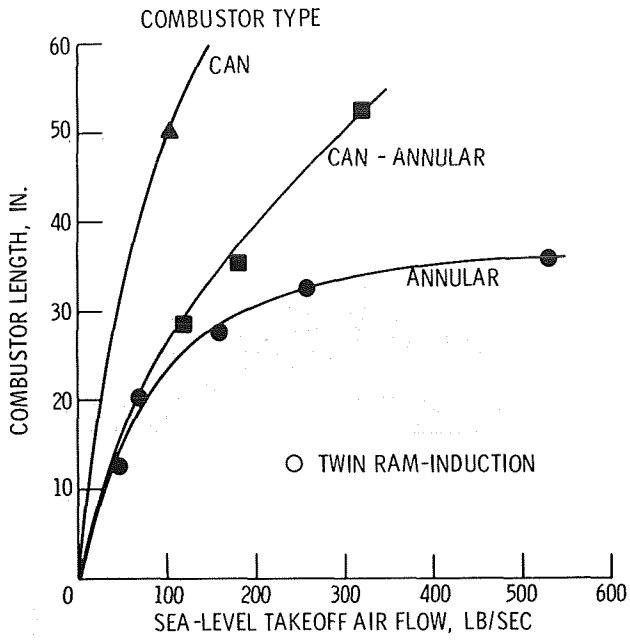

Figure 15. - Comparison of combustor lengths.

This combustor provided a combustion efficiency at simulated takeoff and cruise conditions (90 psia or 62.2 N/cm^2 total pressure, 600^o F (320^o C) and 1150^o F (620^o C) inlet-air temperature) of approximately 100 percent. The total-pressure loss was 5.2 percent at simulated takeoff and 7.2 percent at cruise. The exit temperature pattern factor (maximum temperature minus average temperature divided by average temperature minus inlet temperature) was excellent (0.23). The circumferential variation of temperature was within 150^o F (83^o C) of the exit average of 2200^o F (1205^o C). Smoke numbers measured at a pressure of 6 atmospheres (60.6 N/cm^2) were less than 1.

Tests and development of this combustor are continuing to reduce the total-pressure loss, simplify the overall design, and investigate the performance at higher values of exit temperature.

TURBINES

Current turbine research falls into two general categories, turbine cooling to permit high gas temperatures and turbine aerodynamics to obtain good performance at high loadings.

Turbine Cooling

Ever since the introduction of the gas turbine engine as an aircraft powerplant during World War II there has been a steady increase in the average turbine-inlet temperature with attendant increased engine performance. Until about 1960 the increases in turbine-inlet temperature were realized via improved high-temperature turbine materials. However, in the past decade the incorporation of turbine cooling has augmented metallurgy's contributions to increased operating temperatures.

The early cooled engines incorporated relatively simple cooled airfoil designs, using either single, double, or triple pass convection cooling schemes that were sometimes augmented with film cooling in the leading or trailing edge regions (see refs. 14 and 15 for examples). As the turbine-inlet temperature is increased, convection cooling methods often require such large amounts of cooling air that more effective cooling schemes may need to be employed. Currently, very sophisticated turbine blade configurations employing combinations of convection, impingement, and film cooling are being developed and, as engine temperatures and pressures continue to rise, transpiration cooling becomes of interest.

The Lewis Research Center has a comprehensive program on gas turbine engine cooling underway. Included are both in-house and contract work of a fundamental and applied nature. Engine and cascade facilities are available for tests up to 2500^o F (1370^o C) and new facilities are being designed for tests at higher temperatures.

Film Cooling. Film cooling has been incorporated in cooled turbines by various engine manufacturers, and it has been used in blades investigated experimentally at Lewis many years ago.[15] Generally, film cooling has been used primarily to cool the leading- and trailing-edge regions of turbine airfoils; however, it could be employed around the entire airfoil as shown in figure 16(a). With modern machining methods a very large number of small holes of varying size and at controlled angles could be provided in the airfoil wall at a tolerable manufacturing cost. Film cooling can also be employed to cool other turbine or engine components such as the turbine outer shroud, combustor transition ducting, or exhaust nozzle walls.

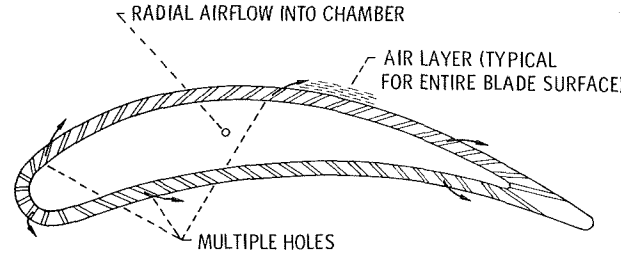

(A) FILM COOLED.

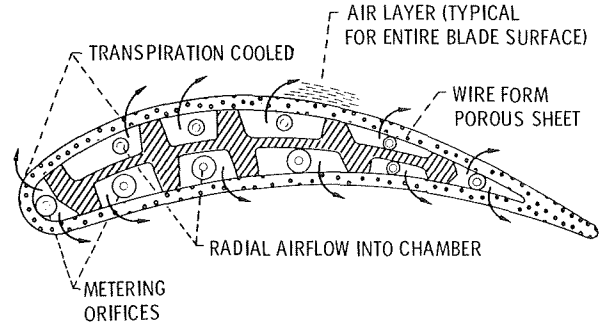

(B) TRANSPIRATION COOLED.

Figure 16. - Turbine blade configurations.

Despite its employment in production engines, film cooling is not thoroughly understood with regard to the fundamental behavior of cooling air films in the presence of high-velocity gas streams. Therefore, Lewis is supporting fundamental studies of film cooling under contract to the University of Minnesota. This work[16,17] indicates that injection into a turbulent air stream at an acute angle yields higher cooling effectiveness than injection at right angles. For high blowing rates, the film cooling effectiveness for a row of holes cannot be predicted from single hole injection data. For the jets from a row of holes, there is less area available for the mainstream gas to flow around and under the jets than for a single jet. As a result, the row of jets is more effective.

Transpiration Cooling. Transpiration cooling, as illustrated in figure 16(b), involves the use of a porous wall that contains thousands of small passages or pores throughout the material. As the cooling air flows through the wall, it first removes heat from the wall by convection. After the air leaves the wall it forms a thin layer of coolant immediately adjacent to the airfoil surface. This layer of coolant separates the wall surface from immediate contact with the high-temperature combustion gas and effectively provides an insulation on the airfoil surface. The insulating effectiveness of this air layer is reflected as a reduction of the hot gas-to-wall heat-transfer coefficient to a fraction of that for a convection cooled blade for equal gas and airflow conditions.

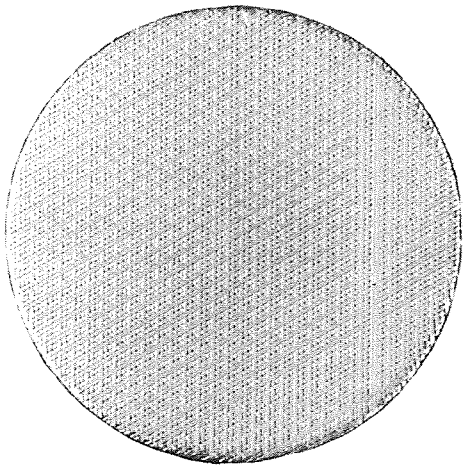

(A) WIRE-FORM POROUS MATERIAL.

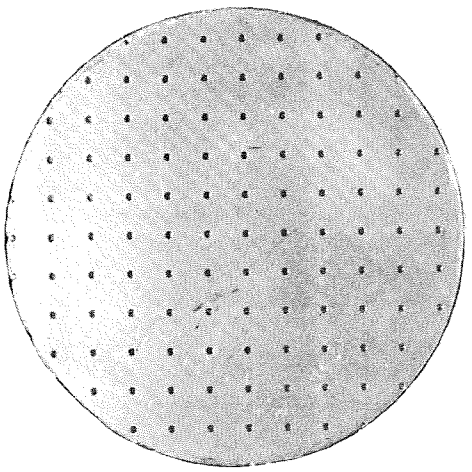

(B) MULTIPLE-HOLE POROUS MATERIAL.

Figure 17. - Surfaces of porous materials.

The porous wall of the blade sketched in figure 16(b) is made from a wire-form porous material, the surface of which is shown in figure 17(a). This material is fabricated by winding flattened wire over a removable mandrel, rolling it to the desired permeability and thickness, and sintering it to provide structural integrity. The porous material is attached to a supporting strut, which in this example (fig. 16(b)) forms 10 compartments within the central core of the blade. Because the wire-form material is of constant permeability, orifices are located in the base of the blade to meter air to each of the compartments to provide for the varying cooling requirements and external pressure field around the blade periphery.

The principal problem in applying transpiration cooling to turbine blades or vanes has been the susceptibility of the porous materials to flow restriction because of oxidation. Once significant oxidation starts, the metal temperature rises and further accelerates the oxidation and flow restriction process.

An obvious method of alleviating the oxidation problems is to increase the pore sizes and decrease the number of pores. However, this involves a departure from ideal transpiration cooling and a possible reduction in cooling effectiveness. Figure 17(b) shows such a material. This multiple-hole material might be called either a pseudotranspiration cooled material or full coverage film-cooled material.

A comparison of the oxidation characteristics of wire-form and multiple-hole porous sheets of the same permeabilities and fabricated from the same nickel-base material (Hastelloy X) is shown in figure 18. After 600 hours exposure in air at 1800° F (980° C) the multiple-

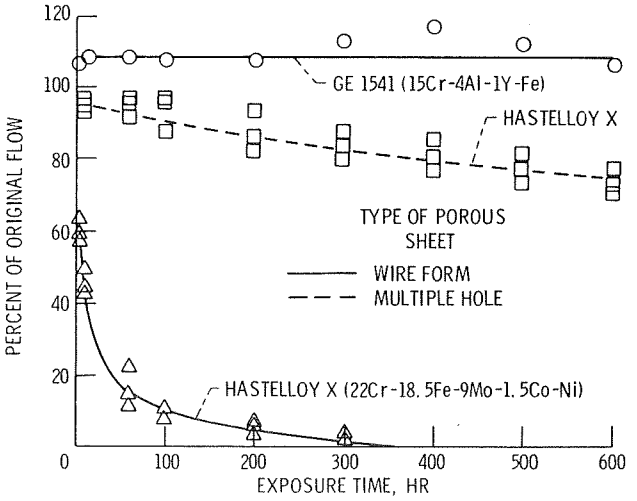

Figure 18. - Improved oxidation resistance in transpiration materials. Temperature, 1800° F.

hole material still retained about 75 percent of its original flow, whereas the wire-form material showed complete flow obstruction in 360 hours at 1800° F (980° C). Also presented in figure 18 are flow data on wire-form specimens fabricated from GE 1541 (iron - chromium - aluminum - 1 percent yttrium) alloy after various oxidation exposures. The GE 1541 material showed no flow reduction after 600 hours exposure at 1800° F (980° C) and represents a significant advance in the state of the art of transpiration cooling at elevated temperatures.

The wire-form porous material using GE 1541 wire was developed by the Filter Division of the Bendix Corporation under a NASA contract. The main fabrication problem involving sintering of the GE 1541 wires. The wires have an extremely adherent oxide which not only protects them against further oxidation but makes sintering very difficult. However, Bendix was able to develop a process for producing good sinter bonds in porous material made from GE 1541 wire.

As with film cooling, the fundamentals of transpiration cooling are not fully understood. For the past 3 years, Professor Kays of Stanford University has been investigating the turbulent boundary layer on a porous plate under a NASA grant. Probably the most significant finding useful to design of transpiration-cooled turbine blades is that his experimental results for uniform blowing rate, plate temperature, and stream velocity agree well with the analytical predictions of reference 18.

Impingement Cooling. The preceding cooling methods essentially reduce the heat flux through the outer surface of the vane or blade; that is, reduce the gas-to-wall heat-transfer coefficients. Additional cooling can be achieved if increased heat-transfer coefficients can be obtained on the inner surface of the walls. In convection cooling this increase of the wall-to-coolant heat-transfer coefficients is conventionally obtained by increasing the heat-transfer surface area through the addition of fins. A relatively new way of further increasing the wall-to-coolant heat-transfer coefficients is to direct one or more jets of cool air onto the surface to be cooled; that is, impingement cooling. This cooling method is finding almost universal acceptance for leading-edge cooling.

Figure 19 shows an impingement cooled blade. The leading edge is cooled directly by a row of circular jets. The inner suction and pressure surfaces are cooled by the impingement of arrays of circular jets; the upstream jets, after impingement, flow along the inner wall surfaces and form a crossflow through which the downstream jets must flow.

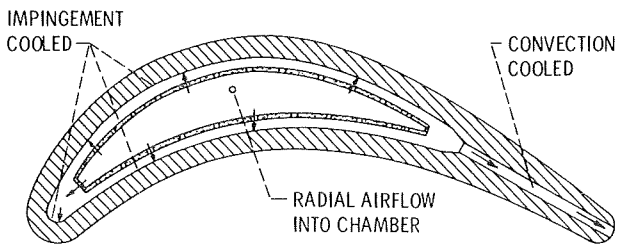

Figure 19. - Impingement cooled turbine blade configuration.

The Lewis Research Center has designed a horizontal finned blade and an all impingement cooled blade for tests in the turbine engine test rig. In the midchord region of the blade, the blade-to-coolant heat-transfer coefficients for the impingement cooled blade were almost twice as high as those for the horizontal finned blade. Depending upon the application under consideration, the wall-to-coolant heat-transfer coefficient for a single jet impinging on a flat surface can be on the order of five times that obtained with conventional convection cooling.

Experimental studies of the fundamentals of flow and heat transfer from impinging jets have been made by NASA. References 19 and 20 report the flow characteristics of a single jet impinging on a flat surface, information which is necessary before adequate heat-surface correlations can be developed for turbine vane or blade design. These and other studies indicate that impingement cooling heat-transfer coefficients can be maximized by a careful selection of geometrical factors such as (1) circular jet nozzle diameter or slot jet width, (2) spacing between jets, (3) spacing between nozzle and impingement surface, etc.

Turbine Aerodynamics

Two aspects of turbine aerodynamics research are currently receiving attention at Lewis: (1) the influence of cooling air discharge on aerodynamic performance of the turbine, and (2) high blade loading.

Cooled Turbine Aerodynamics. Not only must the cooling effectiveness of the various turbine cooling methods be evaluated as discussed in the previous section, but also the influence of the cooling air on the aerodynamic performance of the turbine must be understood to be properly factored into the turbine and engine performance assessment. Accordingly, an effort is under way at Lewis to determine the effects that various cooling methods have on turbine aerodynamic performance. A photograph of three example cooling schemes tested

C-70-447

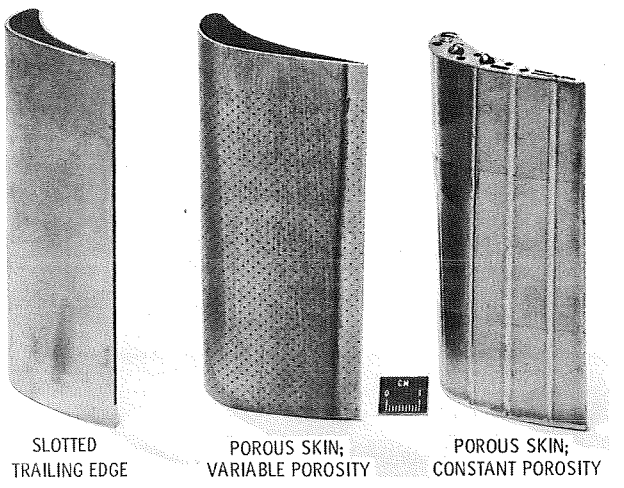

Figure 20. - Example stator vanes tested.

is shown in figure 20. All stator vanes shown have the same outer blade profile but differ in the manner of ejecting the simulated coolant into the main gas stream. The first vane ejects the coolant through a continuous slot along the trailing edge in a direction generally the same as the primary gas. The other two are of the transpiration type, where the coolant oozes through a porous skin in a direction generally normal to the main gas stream. The stator vane in the middle has a self-supporting skin that has a variable porosity around the blade surface. The other transpiration vane on the right is made by wrapping a constant porosity wire mesh around an internal strut and welding as indicated. Flow is varied by the use of metering orifices shown on the end cap. Stage tests were conducted using a full annular stator vane assembly made of each particular blade shown in conjunction with a common rotor. The effect of the manner of ejecting the coolant air on turbine efficiency for the first two vanes tested is shown in figure 21. Ejection through the trailing edge in the direction of the main flow had little effect on efficiency. In

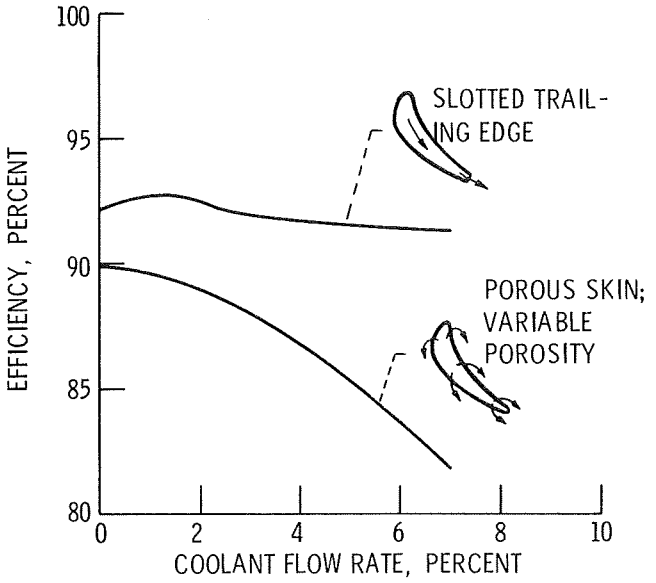

Figure 21. - Effect of coolant type on efficiency.

fact, about 1 percent coolant caused a slight increase in thermodynamic efficiency because of the reduction of the effective thickness and loss of the blade trailing edge by the coolant. However, the efficiency of the variable porosity transpiration-type vane is considerably lower. For example, at a coolant flow rate of 3 percent, it is 4 points lower. Surveys made behind each blade row tested indicated this large difference to result primarily from a thickening of the boundary-layer buildup caused by the interaction of the coolant and primary air along the suction, or convex, surfaces of the transpiration-type blade. Tests are presently being conducted with the wire-mesh-type blade shown on the right in figure 20. Although the tests described do not include actual cooling and consequent internal blade losses caused by intricate flow passages, relative comparisons of the results have value in an understanding of the net effect of the coolant on the aerodynamics of the combined flows. The work described is covered in more detail in references 21 to 25. Future tests will be conducted in a multistage turbine to determine the effect of the coolant ejected from the first-stage stator vanes on succeeding blade row performance.

Highly Loaded Turbine Blades. Approaches in turbine design to decrease size and weight include reduction of the number of stages, the turbine diameter, and the number of blades per stage. These reductions increase the loading of the remaining stages and blades. Higher blade loading, which is similar to wing lift force, is normally attained by increasing the pressure difference between the convex and concave blade surfaces. Unfortunately, this can result in high flow deceleration on the blade surface and cause the flow to separate from the blade with high turbulence and loss. Accordingly, both plain blades and unconventional blade concepts are being studied in an attempt to increase blade loading to higher limits and still maintain high efficiency. Two concepts that have shown promise are the tandem and the jet-flap blades. A rotor using each type of blade is shown in figure 22. Both are boundary-layer control devices to permit higher blade loading while preventing flow separation. The tandem blade does not require a secondary gas, while the jet-flap blade does. This fact suggests using the jet-flap blade in a cooled turbine application, where the coolant would eject through the jet into the main gas stream.

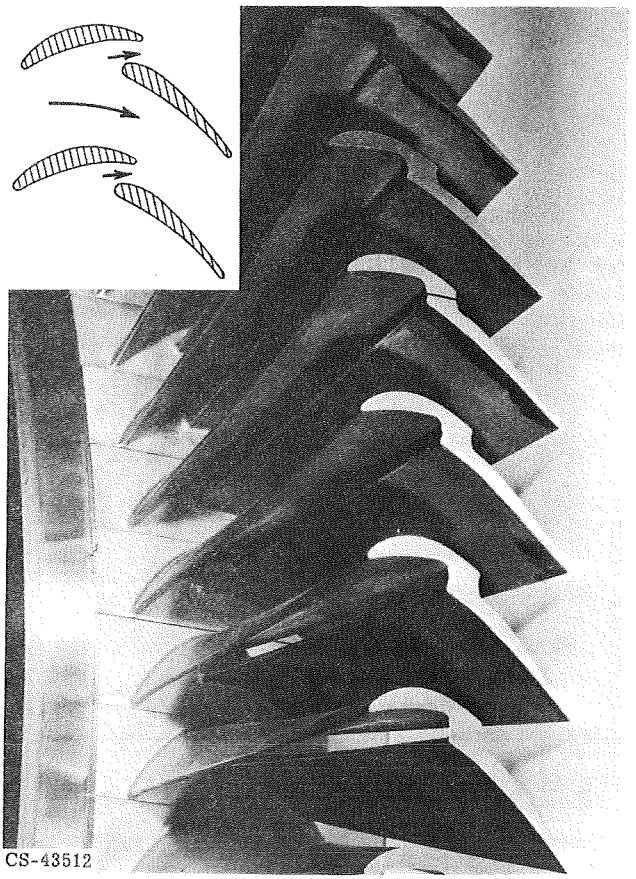

(A) TANDEM BLADE.

Figure 22. - High blade loading rotors.

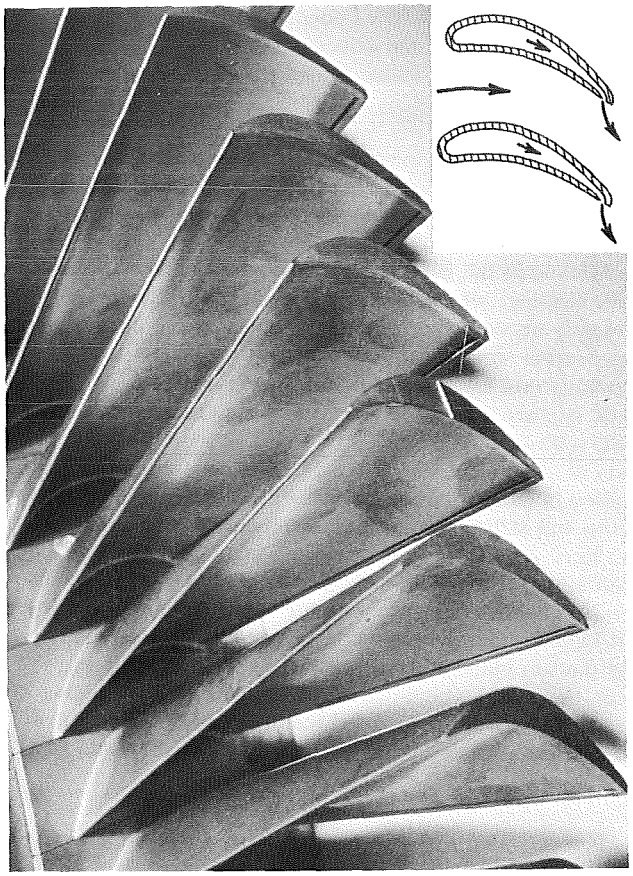

(B) JET-FLAP BLADE.

Figure 22. - Concluded. High blade loading rotors.

Two- and three-dimensional cascade tests and rotating stage tests have been conducted at Lewis and under contract with the Allison Division of General Motors.[26-28] The results of four-stage tests using a plain bladed rotor, a jet-flap rotor, and two tandem bladed rotors are shown in figure 23. Efficiencies of the four turbines are plotted as a function of a blade loading factor. The solidities of the four blades were varied to change the severity of loading, with the lowest solidity rotor representing the fewest blades and highest loading. The results (fig. 23) show that the group of three rotors at loading factors between 0.8 and 1.0 yielded turbine efficiencies of about 89 percent. As loading was increased to a factor of 1.5, the efficiency of the tandem rotor 2 decreased about 3 points to a value of 86 percent. This significant penalty indicates that further effort is required at the higher loadings to evaluate the merits of the use of the more complicated advanced blade concepts. Comparable tests will be conducted at Allison for a jet-flap blade designed at the higher loading condition.

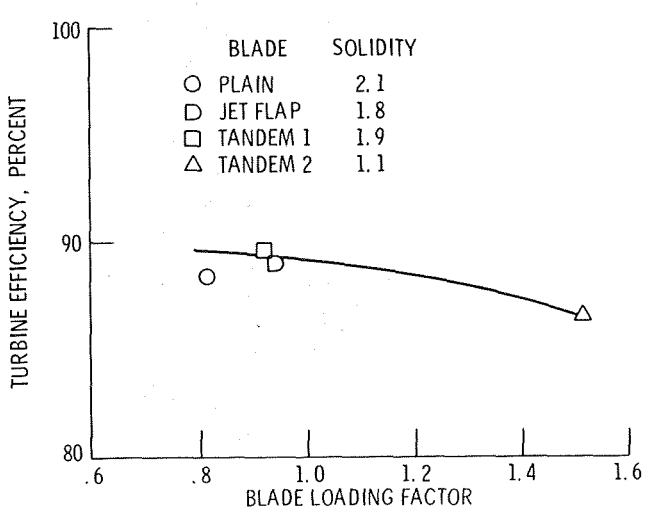

Figure 23. - Performance of turbines with highly loaded blades.

TURBINE ENGINES

Much attention and effort is currently being devoted by engine companies and government organizations to the engine stall problem, which is particularly critical for the modern high-performance afterburning turbojet and/or the turbofan engine installed in high-speed - high-altitude aircraft. Some of the Lewis Research Center effort to understand the flow phenomenon of stall and, thereby, to improve the compressor stall margin has been discussed previously in the component section, Fans and Compressors. In addition to these component studies, an extensive program utilizing complete turbine engines has been instituted to investigate the stall phenomena with the objective of establishing a more detailed understanding of the steady-state and dynamic flow processes and attendant component interactions. High response instrumentation and specialized testing techniques have been developed and some research has been conducted utilizing the J85, TF30, and GE-1/10 engines. The methods and test procedures utilized in this program and a few of the results obtained with the TF30 engine are described.

Engine Installation

The TF30 is a two-spool afterburning turbofan engine having a three-stage fan. It was installed in an altitude chamber in conventional direct connect fashion. The altitude chamber included a forward bulkhead which separated the inlet plenum from the test chamber (fig. 24). Conditioned air was supplied to the plenum at the desired pressure and temperature. It flowed from the plenum through a bellmouth and inlet duct to the engine. A high-response bypass valve located in the bulkhead allowed some air to bypass the engine and was automatically controlled to maintain a constant inlet pressure and ram pressure ratio across the engine during both steady-state and transient engine operation. The exhaust from the engine was captured by a collector extending through a rear bulkhead and discharged into the facility exhaust system wherein the exhaust pressure was maintained constant at the desired altitude by automatically controlled valves.

Engine Instrumentation

The layout of the high-response compressor pres-

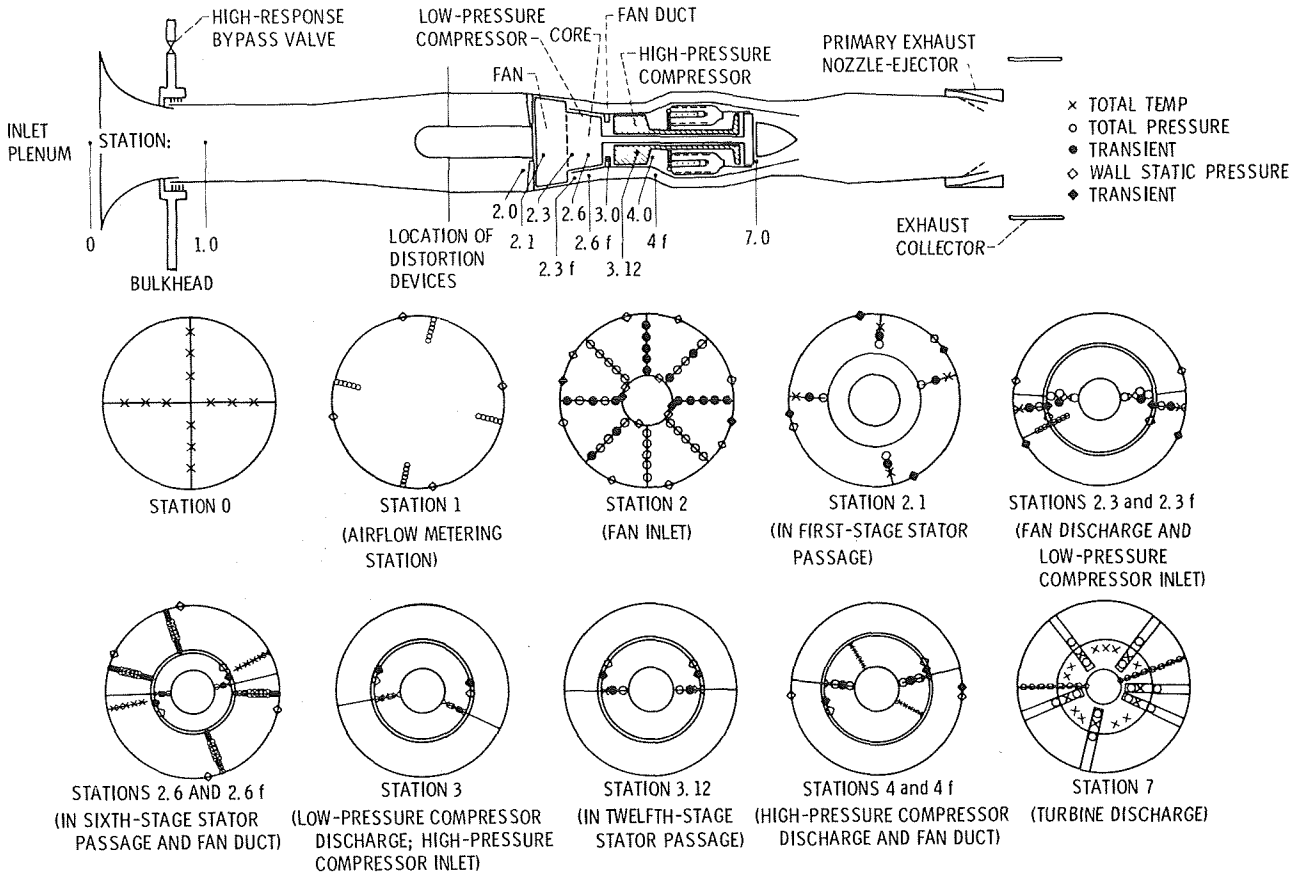

Figure 24. - Instrumentation layout.

sure instrumentation is shown in figure 24. There were also high-response pressure measurements in the combustor, fan duct, and afterburner, as well as conventional steady-state instrumentation throughout the engine. The fan inlet rakes comprised 40 high-response total-pressure measurements. All the other compressor high-response instrumentation consisted of two pairs for total and static pressures located approximately 180° apart installed at each of the stations indicated in figure 24. The pressure transducers, which were mounted in a water-cooled jacket to eliminate calibration changes due to temperature, were recalibrated in place prior to recording data. The high-response data were recorded simultaneously on a high-speed digitizer recorder and on magnetic tape. Details of the instrumentation and calibration techniques are discussed in references 29 and 30.

General Test Procedure

The investigation was conducted at a Reynolds number index (i.e., Reynolds number relative to standard sea-level conditions) of 0.5 with an inlet temperature of 60° F (16° C), which resulted in an inlet total pressure of 7.5 psia (5.2 N/cm^2). The ram pressure ratio across the engine was held constant at 3 to assure a choked exhaust nozzle for all operating conditions. These test conditions correspond to a range of flight conditions representative of the flight regime of a supersonic aircraft.

To determine the engine stall margin when operating with no inlet distortion or with fixed distortion introduced by screens, the following techniques were employed to induce stall in the three compressor units (fan, low-pressure compressor, and high-pressure compressor): The low-pressure compressor operating line was raised toward the stall limit by increasing the exhaust nozzle area above the rated area; the engine was then very slowly accelerated (10 to 20 rpm/sec) until the engine either stalled or reached one of its operating limits. In a similar manner the exhaust nozzle was closed to raise the operating lines of the high-pressure compressor and fan unit, and again a slow acceleration was made until stall occurred in one of these units or an engine operational limit was reached. The slow acceleration was used to keep the engine close to the steady-state operating line for the particular exhaust nozzle area being employed. Data from the transient instrumentation were recorded during these slow accelerations until some time after the engine had stalled. A second method of inducing stall in the high-pressure compressor was to inject an increment of fuel into the engine fuel system, which would cause a step increase in pressure at the high-pressure compressor exit. The size of the fuel step was then successively increased until stall was encountered in the high-pressure compressor. Stall data were obtained over a range of rotor corrected speeds from idle to maximum.

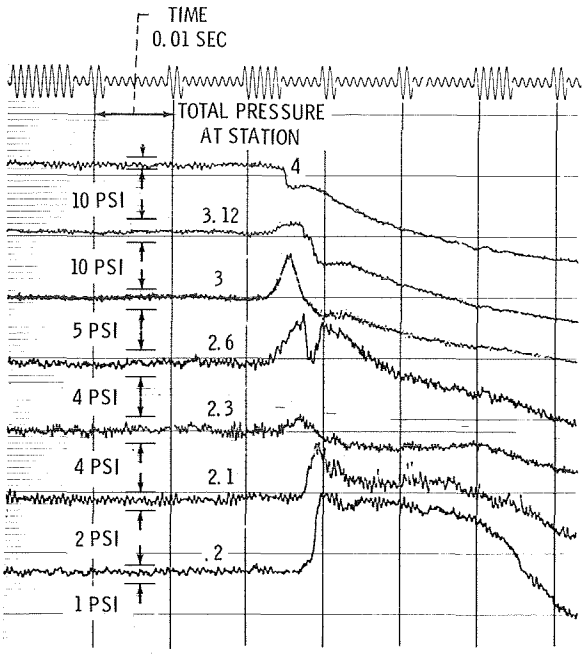

Figure 25. - Typical time histories during stall transient of YTF30-P-1 turbofan engine at Reynolds number index of 0.5. High-pressure compressor stall; high-pressure rotor speed, 97 percent; exhaust-nozzle area, 78 percent rated area.

Typical time histories of pressures in the compressors for one observed stall are presented in figure 25 for the case of a slow acceleration to a high-pressure compressor stall with a small exhaust nozzle area (78 percent of rated area). Figure 25 shows a simultaneous rise in $P_{T,3.12}$ (12th stage) and a drop in $P_{T,4}$ (16th stage or compressor exit) indicating that the stall originated between those locations. The progression of the stall forward through the compressors can be seen.

It is possible to use data such as these to determine the stall pressure ratio of stages ahead of the stage that stalls initially. This method is based on the fact that, as the first stage stalls, its flow is reduced so rapidly that the pressure at the exit of the preceding stage will rise before the inlet pressure of that stage is affected. Thus, this stage in turn stalls, and the process is repeated until the stall has progressed completely through the compressor to the inlet.

Special Techniques and Results

Four special distortion techniques that have been or are about to be employed in this program are pressure distortion jets, temperature distortion device, choked inlet duct, and compressor discharge inflow bleed. The pressure jet distortion system has been employed to produce both steady-state distortions and fluctuating pressures in the inlet duct ahead of the engine. The engine effects obtained when producing steady-state distortions with the jets were practically identical to those obtained when using screens, but testing was greatly facilitated by use of the jets.[31,32] The temperature distortion device consists of a large ($5\frac{1}{2}$-ft or 1.7-m diam.) hydrogen burner mounted in front of the engine inlet bellmouth and has the capability of producing steady-state circumferential and radial distortions or providing temperature ramps as high as 10 000° F (5550° C) per second. The choked inlet duct is similar to the device used by Kimzey[33] and has the possibility of simulating the environment provided by some aircraft inlets. The fourth technique involves reversing the flow in the compressor discharge ports and hence the name "compressor discharge inflow bleed." It, of course, requires an external source of high-pressure air but has the advantage of permitting a gradual approach to the stall limit of the high-pressure compressor at high corrected speeds without overheating the turbine.

The arrangement of the pressure jet system nozzles in the engine inlet duct is presented in figure 26. In this

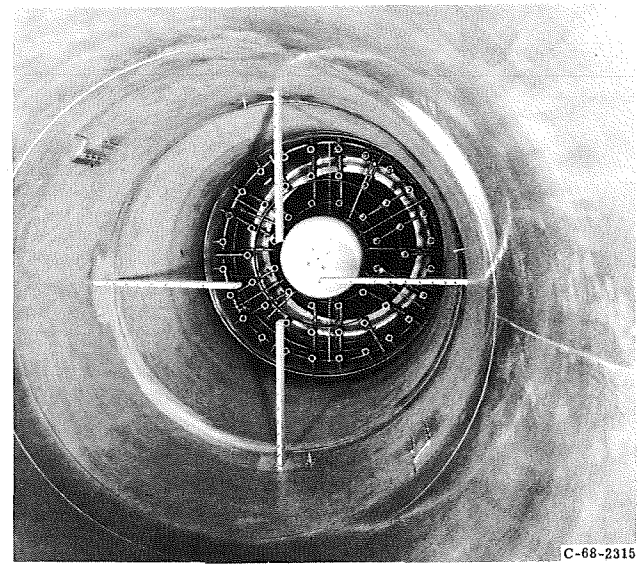

Figure 26. - Pressure jet stream installed in engine inlet duct (view looking toward engine inlet).

system, secondary jets of air are injected counter to the primary airflow in the engine inlet duct forward of the compressor face. Through control of the secondary-air distribution and flow rate, variable amplitude steady-state or dynamic pressure distortions or uniform dynamic pressure oscillations can be produced. As can be seen in figure 26, the secondary jet nozzles are uniformly distributed circumferentially and radially in a pattern that repeats every 60° of circumferential extent. Six high-response servo-operated valves, designed especially for this application, are employed to control secondary airflow to each 60° segment. Momentum interchange between the secondary and primary streams occurring upstream of the jet nozzle array is primarily responsible for the total-pressure loss that is generated. The amount of total-pressure loss incurred is controlled by varying the secondary airflow. If it is varied in a pulsating manner, then a pulsating pressure is generated at the engine face.

A plot of some of the individual pressure measurements at the engine inlet face as a function of time is presented in figure 27 for a pulsation frequency of 10 hertz. All the individual pressure measurements are in phase and about equal in amplitude, and a reasonable approximation to a sine wave was obtained. Some of the engine performance data obtained when pulsating the inlet at this frequency (10 Hz) are presented in figure 28,

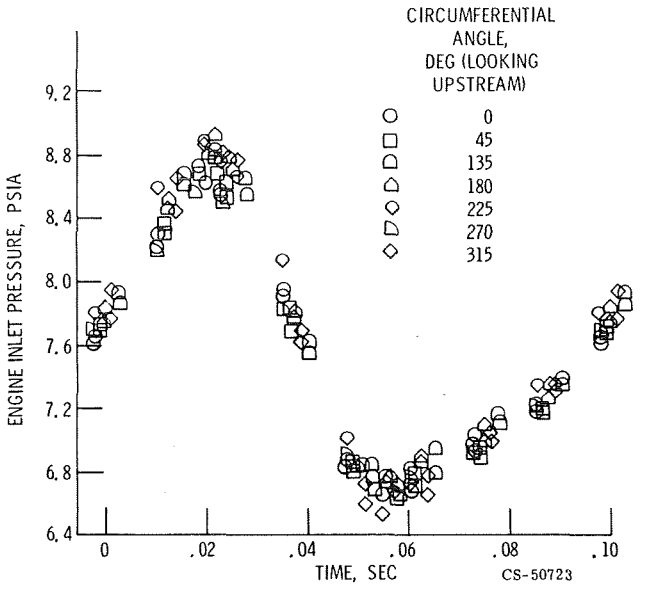

Figure 27. - Variation of engine inlet pressure with time. Input frequency, 10 hertz.

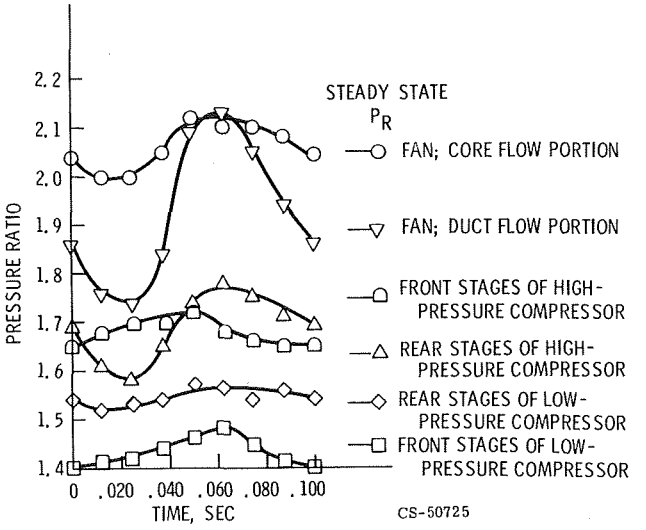

Figure 28. - Variation of stage group pressure ratios during uniform inlet pressure variations. Corrected engine speed, 87 percent; input frequency, 10 hertz; $\Delta P_{T,2}/P_{T,2}$, 0.284.

which shows the variation of a number of compressor interstage pressure ratios as a function of time for an average steady-state inlet total pressure of 7.4 psia and 87 percent corrected speed. The significant pressure-ratio curves are for the stage groups immediately adjacent to a large volume; namely, the outer portion of the fan and rear stages of the high-pressure compressor. Not only do these two stage groups go through a much greater pressure-ratio variation than the others, but also their swing above their steady-state value of pressure (indicated by the short horizontal line on the right and measured just prior to onset of the pulsation) is significantly greater than below it. The data presented in figure 28 were obtained at an amplitude just slightly less than that required to stall the compressor and are considered to be typical of conditions just prior to stall. Examination of the analog traces at the stall point indicated that the stall originated in the back end (stages 12 to 16) of the high-pressure compressor even though the pressure-ratio excursion across the fan tip was greater. Apparently the fan has more stall margin than the high-pressure compressor. Data such as these are further discussed in reference 34.

In order to summarize and compare the effects of various modes of distortions on the engine stall limits, the results are presented in figures 29 and 30 on coordinates of stall tolerance parameter $(P_{T,av} - P_{T,min})/P_{T,av}$ and input frequency. The term $P_{T,av}$ is defined as the average pressure between $P_{T,max}$ and $P_{T,min}$; $P_{T,max}$ and $P_{T,min}$ are the maximum and minimum inlet pressures which occurred prior to stall for over a 2-millisecond time period. The 2-millisecond time period was selected as significant because it represents the approximate time for the fan - low-pressure compressor to rotate 90° at the rotor speed for which the data are shown. Stall margin is relatively insensitive to circumferential distortion extent above 90°, while at values well below 90° substantially greater distortions can be tolerated. Stall tolerance parameter is defined in this manner for the distorted inlet-pressure data because the resulting parameter is a measure of the instantaneous distortion (subject, of course, to the 2-millisec criterion). Thus, if instantaneous distortion were the sole factor in determining stall, all modes and frequencies of inlet-pressure variations should produce stall at the same value of stall tolerance parameter.

Figure 29 compares the stall tolerance parameter for the 180° steady-state distortion, the 180° pulse distortion, and the 180° oscillating distortion. The first two distortion modes are not related to frequency and

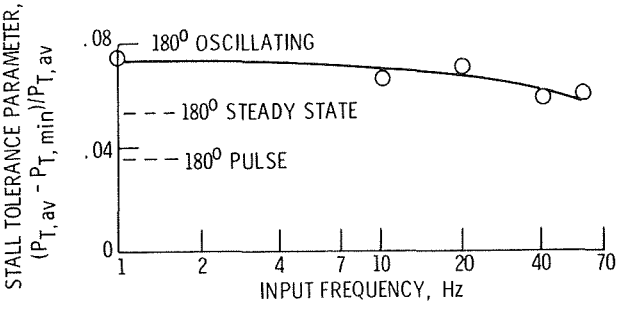

Figure 29. - Comparison of effects of steady-state, oscillating, and pulse 180° distortions on stall tolerance.

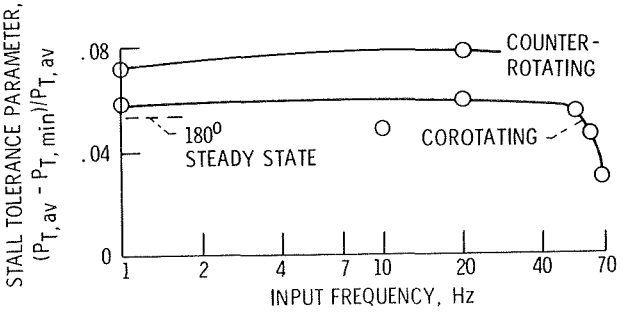

Figure 30. - Comparison of effects of rotating and 180° steady-state distortions on stall tolerance.

are indicated at the left of the figure. Stall was encountered at a stall tolerance parameter of 0.054 with the steady-state distortion as compared to 0.036 when the pulse distortion was imposed, thus indicating that the rate of onset of a distortion has a significant effect on the engine tolerance to the distortion. The oscillating distortion produced some variation in stall tolerance parameter as frequency was varied. At 1 hertz the value was 0.073, and it decreased as frequency was varied until a stall tolerance parameter of 0.057 was reached at a frequency of 60 hertz.

Figure 30 compares the stall tolerance parameter for the 180° steady-state distortion and two rotating distortions. When the distortion was a counterrotating type (opposite to the direction of the fan - low-pressure compressor rotor), the stall tolerance parameter was substantially greater than for the steady-state distortion or for the corotating distortion. At 20 hertz the value of stall tolerance parameter was 0.078 for the counterrotating distortion, as compared to 0.059 for the corotating distortion. The steady-state distortion value as previously stated was slightly over 0.054. As the frequency of the corotating distortion was increased, the stall tolerance decreased. As the frequency approached 72 hertz (i.e., one-half of the fan - low-pressure compressor rotor speed), the stall tolerance parameter decreased to about 0.030, which is slightly below the value attained for the 180° pulse distortion. This substantial decrease in stall tolerance parameter with frequency strongly suggests that stall tolerance is a function of the dwell-time of the fan-compressor rotor blading in the low-pressure region of an engine-inlet distortion. It is expected that results from this continuing investigation will contribute to a better detailed understanding of the engine stall mechanism and the effects of steady-state and dynamic distortions thereon.

INLETS AND NOZZLES

Many different inlet and nozzle designs can be considered for supersonic aircraft, and their proper selection is a complex decision that depends on overall aircraft design and mission requirements. Some of the factors in this decision were discussed in the 1968 ICAS meeting.[4] Since that time additional inlet and engine tests have been completed in the Lewis 10- by 10-Foot Supersonic Wind Tunnel, and several transonic flights of an F-106 aircraft have been made as an in-flight test facility. Representative results have been selected from these programs to illustrate research objectives and progress.

Inlets

Although external supersonic compression inlets have been used on the majority of existing aircraft, there is a strong interest in using mixed external and internal compression for aircraft requiring sustained flight at speeds of Mach 2.5 or higher. As illustrated in figure 31, a mixed-compression design provides the external supersonic compression ahead of the cowling, and the internal compression occurs between the cowl lip and the throat. To obtain high performance, the terminal shock is positioned close to the throat, but if a disturbance displaces this shock ahead of the throat, it is violently expelled with a large drop in pressure and flow rate into the compressor. The principal reason for selecting this compression mode is to reduce the cowl drag; however, the inlet becomes more sensitive to angle-of-attack effects and its control system becomes more complex in order to prevent the flow instabilities associated with this unstart phenomenon.

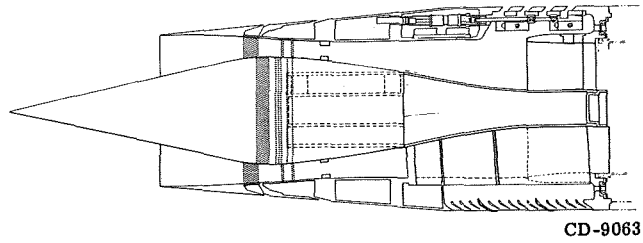

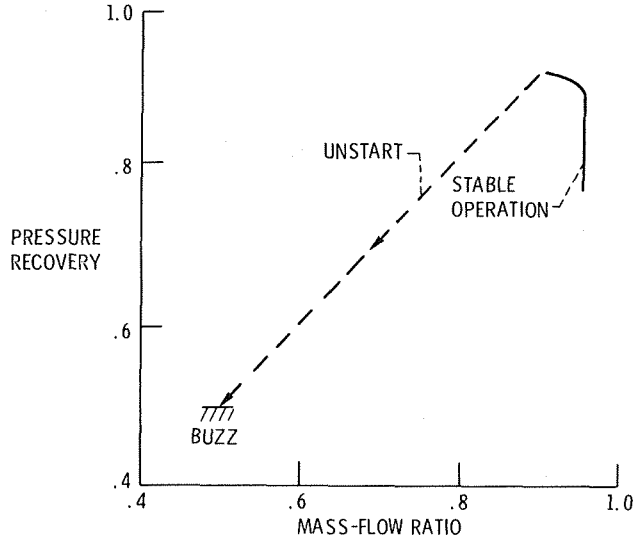

Figure 31. - Mixed compression inlet.

The effects of an unstart on engine operation will vary depending upon the severity of the flow transient and the initial stall margin of the compressor. A mixed-compression inlet designed for Mach 2.5 was tested recently with a J85 turbojet engine[35-38] to evaluate these effects. The loss in compressor-inlet pressure due to the unstart transient would cause a rapid increase in the instantaneous compressor pressure ratio, which would tend to drive it toward the stall line. This transient was relatively mild at Mach 2.0, and its effect on the engine operation is summarized in figure 32. If the initial compressor pressure ratio was low enough that the transient peak did not exceed the steady-state stall line, the compressor did not stall and engine operation remained normal. If the initial pressure ratio was high enough that the transient peak just reached the stall line, the compressor stalled and recovered quickly, but if it exceeded the stall line, both stall and combustor blowout occurred and the engine could not recover. Although the inlet unstart transient was very rapid, the steady-state stall line was a useful parameter in predicting the resulting behavior of this particular engine. The unstart transient at

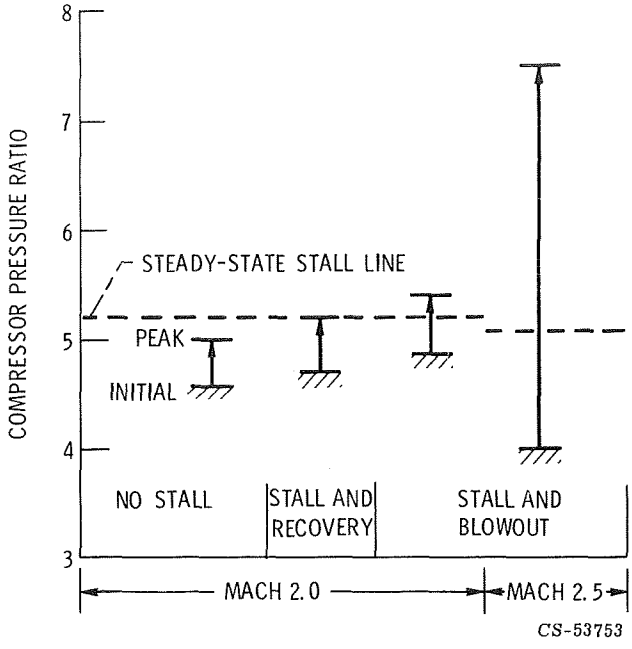

Figure 32. - Inlet unstart effect on engine.

the design Mach number of 2.5 is also shown on the figure. In this case the transient was so severe that there was no possibility of preventing stall even though the initial stall margin was quite large.

Accordingly there is a strong motivation to improve the inlet design to minimize the possibility of an unstart occurring. One approach is to develop high-speed, closed-loop inlet controls.[39] An alternative technique is to improve the design of bleed systems in the region of the throat (indicated in fig. 33) so that if the shock is pushed ahead of the throat, large amounts of air can be spilled without causing an unstart. However, with the usual bleed system design (using fixed-exit areas), excessive quantities of air would be spilled during normal operation with the shock downstream of the throat. As illustrated in the figure, a variety of high-speed valves have been tested on a mixed-compression inlet which were designed to close the exit area during normal operation and to open automatically to spill air if the terminal shock was displaced ahead of the throat. One of the valves was a mechanical-free piston device that was positioned by the pressure differentials that occur when the terminal shock is displaced. The other valve used an aerodynamic vortex to restrict the discharge area during normal operation. The pressure changes that result when the shock moves ahead of the throat disrupts the vortex and, hence, larger quantities of air can be spilled. The effects of these valves on the inlet performance characteristics are shown in figure 34. Both valves produced a significant increase in the inlet stability margin without causing any degradation in normal performance. The greater stability provided by the mechanical valves resulted because the flow areas in the open position could be made much larger than those of the vortex valve. It appears that valves such as these can provide a significant increase in mixed-compression inlet stability. Additional effort appears justified in developing improved designs which have a lower frontal area and thus reduced cowl drag.

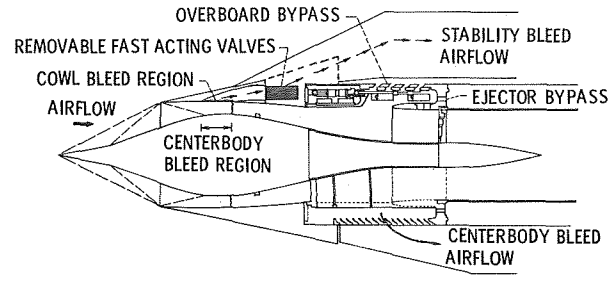

(A) CROSS SECTION OF 60-40 STABILITY INLET.

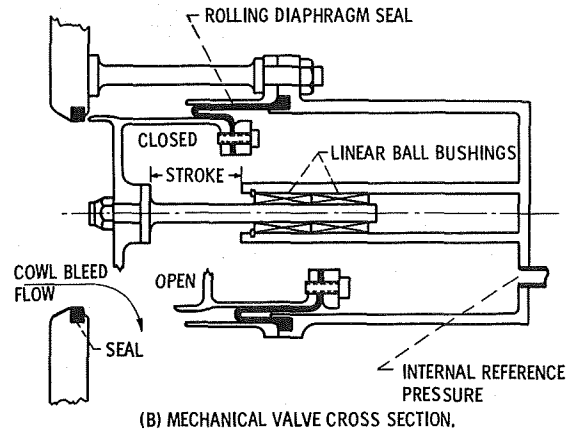

(B) MECHANICAL VALVE CROSS SECTION.

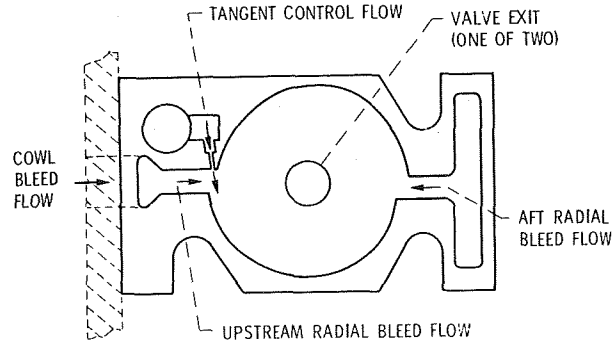

(C) VORTEX VALVE CROSS SECTION.

Figure 33. - Inlet shock stabilization valves.

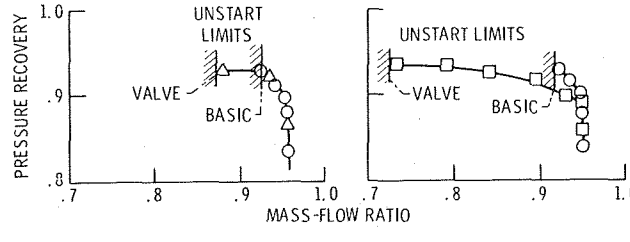

(A) VORTEX VALVE. (B) MECHANICAL VALVE.

Figure 34. - Valve effects on inlet performance.

Nozzles

One of the particularly difficult problems in nozzle design is to provide the large reduction in expansion ratio for acceptable off-design cruise efficiency at transonic speeds. At this speed the nozzle performance is quite sensitive to the external flow field created by the airframe. This installation effect is difficult to evaluate in model tests because of the size limitations of transonic tunnels. Therefore, as illustrated in figure 35, NASA

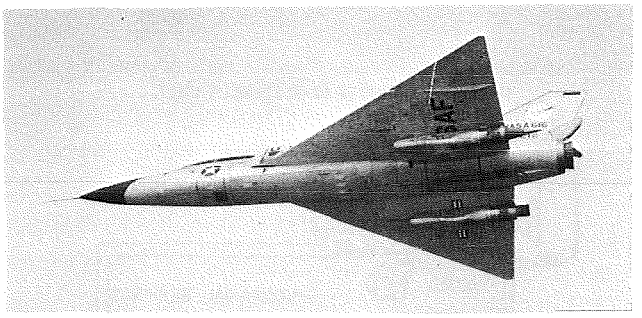

Figure 35. - F-106 transonic propulsion research aircraft.

has initiated a transonic flight test program using a modified F-106 aircraft. A J85 engine pod has been added to each wing, and large variations can be made in the design of its exhaust system. This particular engine installation is of interest for supersonic cruise aircraft since the wing can shield the inlet from angle-of-attack effects.

The nacelle flow field interacts with the wing flow field to create a compression wave (or terminal shock) around the nozzle which tends to improve nozzle performance at flight speeds below Mach 0.95.[40,41] At higher speeds this shock moves further downstream and nozzle performance decreases abruptly. The resulting effect on the performance of a variable-flap ejector is shown in figure 36. (The design of this nozzle is described in

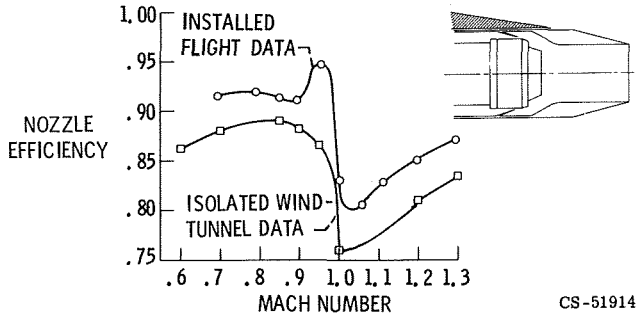

Figure 36. - Installation effect on variable-flap ejector.

ref. 42.) The installed performance was significantly better than that obtained in wind tunnel tests of the isolated nozzle model,[43] particularly at speeds between Mach 0.90 and 0.95. This improvement in nozzle performance was the result of the terminal shock wave on boattail pressures. As shown in figure 37, the installed boattail drag was significantly reduced for those flight speeds which kept the terminal shock ahead of or on the boattail surface. At higher speeds the boattail drag increased abruptly to values near those obtained in isolated

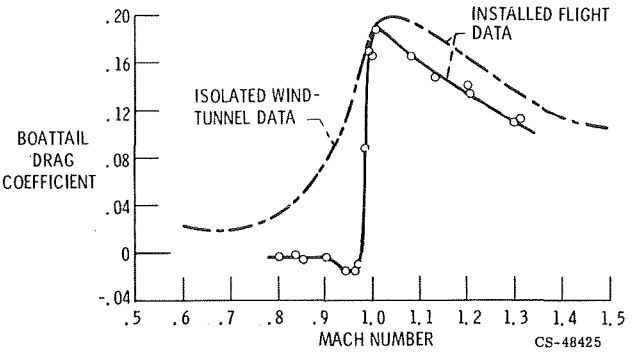

Figure 37. - Installation effect on boattail drag.

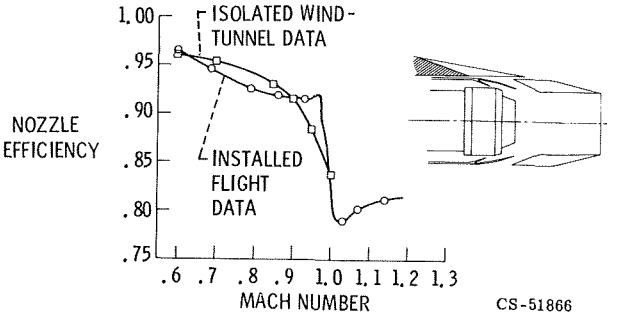

Figure 38. - Installation effect on auxiliary-inlet ejector.

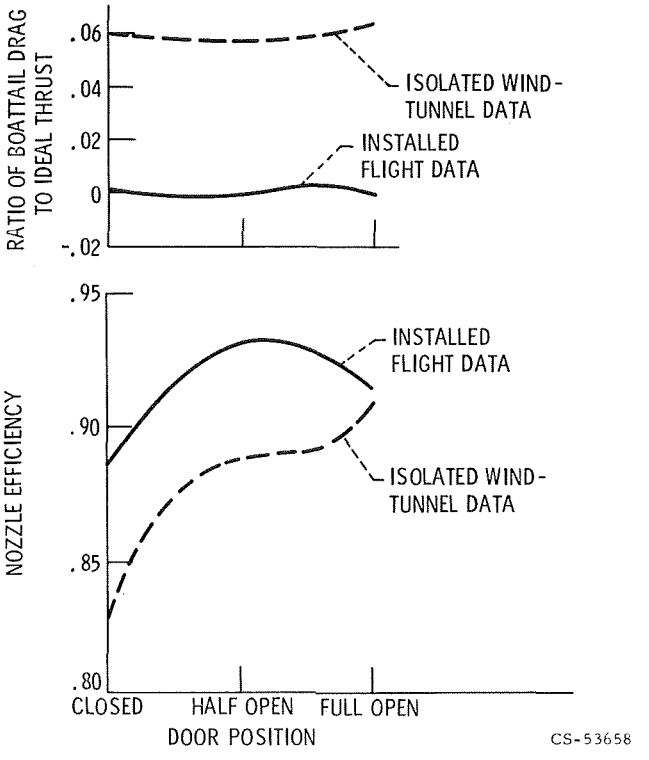

Figure 39. - Effect of door position on auxiliary inlet ejector performance at Mach 0.95.

nozzle tests. Although the details of the afterbody shape had significant effects on the isolated boattail drag, these effects were much less significant when the nozzle was installed on the airframe.

Another nozzle concept that has been flight tested is the auxiliary-inlet ejector illustrated in figure 38. (Design details are given in ref. 44.) The installation effect obtained with floating inlet doors relative to that obtained with the isolated tunnel model was much less significant than that for the variable-flap ejector. The effect of varying the auxiliary inlet area with fixed doors at Mach 0.95 is shown in figure 39. Although the installed boattail drag again was significantly less than that of the isolated tunnel model regardless of door opening, the overall nozzle efficiency did not improve as rapidly when the door opening was increased. It optimized at a partly open position, whereas in isolated tests the full-open position was desired. This loss in inlet effectiveness occurred because the boundary-layer profiles approaching the installed auxiliary inlets were thicker than in isolated model tests and varied around the nacelle circumference.

The installation effect on plug-nozzle efficiency is shown in figure 40. (Details of the design are presented

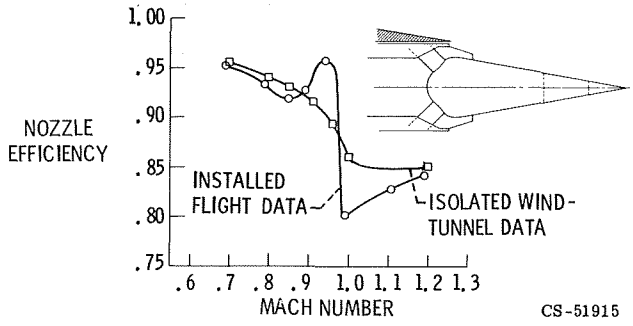

Figure 40. - Installation effect on conical-plug nozzle.

in ref. 45.) This effect was favorable near Mach 0.95, but a sharply adverse effect occurred just above Mach 1.0. Both plug and primary-flap pressure forces are shown in figure 41 for the isolated and installed nozzles. This adverse effect above Mach 1.0 was primarily a result of greater drag forces on the plug surface. Additional tests will be initiated soon with an air-cooled plug so that larger throat areas corresponding to afterburning power settings can be used at these higher speeds. It is anticipated that this adverse installation effects will be less significant at these higher power conditions.

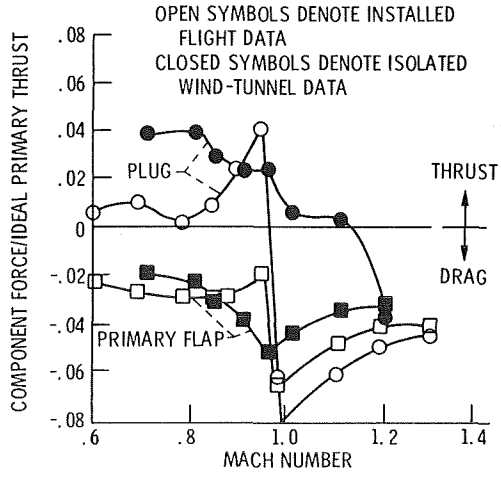

Figure 41. - Installation effect on conical-plug and primary-flap forces.

Although isolated nozzle tests are useful in the early development of promising concepts for a particular application, the installation effects can influence the choice of an optimum configuration. For the podded engine installation used on the F-106 aircraft, this effect raised the performance of the variable-flap ejector (which was the lowest in isolated nozzle tests) so that its performance was more competitive with that of the installed auxiliary inlet ejector and plug nozzle.

CONCLUDING REMARKS

A representative cross section of the research programs of the NASA Lewis Research Center in the turbojet-turbofan propulsion area has been described and some recent results presented. Progress continues in the high-temperature materials area with new improvements in superalloy compositions and processing and with promising developments in composites. Compressor and fan technology proceeds towards higher stage loading and broader operating ranges with improved stall margins. Combustor developments are leading towards shorter units while maintaining high efficiency and good pattern factors. Emphasis in the turbine area is on improved cooling to permit higher gas temperatures and on increased blade loading.

Instrumentation and testing techniques are being improved to investigate the engine stall problem and to obtain a detailed understanding of the phenomenon. The use of fast-acting bleed valves offers promise of providing substantial stability margin for mixed compression supersonic inlets and attendant protection against unstarts and engine stall without degradation of normal performance. A flight investigation of propulsion-system installation problems indicates the importance of interference effects on the selection of optimum configuration of exhaust nozzles.

Significant progress has been achieved in aircraft gas turbine technology and substantial further gains lie ahead.

REFERENCES

1. Silverstein, Abe: Progress in Aircraft Gas Turbine Engine Development. Aerospace Proceedings 1966. Vol. 2. Joan Bradbrooke, Joan Bruce, and R. R. Dexter, eds., Macmillan Co., 1967, pp. 587-605.

2. Freche, John C.; and Hall, Robert W.: NASA Programs for Development of High-Temperature Alloys for Advanced Engines. J. Aircraft, vol. 6, no. 5, Sept.-Oct. 1969, pp. 424-431. (See also paper 68-26, ICAS, Sept. 1968).

3. Roudebush, William H.: State of the Art in Short Combustors. Paper 68-22, ICAS, Sept. 1968.

4. Beheim, Milton A.; and Boksenbom, Aaron, S.: Variable Geometry Requirements in Inlets and Exhaust Nozzles for High Mach Number Applications. Paper 68-20, ICAS, Sept. 1968.

5. Waters, William J.; and Freche, John C.: A Nickel Base Alloy, WAZ-20, With Improved Strength in the 2000° to 2200° F Range. NASA TN D-5352, 1969.

6. Freche, John C.; Waters, William J.; and Ashbrook, Richard L.: Evaluation of Two Nickel-Base Alloys, Alloy 713 C and NASA TAZ-8A, Produced by Extrusion of Prealloyed Powders. NASA TN D-5248, 1969.

7. Petrasek, Donald W.; Signorelli, Robert A.; and Weeton, John W.: Refractory-Metal-Fiber - Nickel-Base-Alloy Composites for Use at High Temperatures. NASA TN D-4787, 1968.

8. Petrasek, Donald W.; and Signorelli, Robert A.: Preliminary Evaluation of Tungsten Alloy Fiber-Nickel-Base Alloy Composites for Turbojet Engine Applications. NASA TN D-5575, 1970.

9. Harley, K. G.; and Burdsall, E. A.: High-Loading Low-Speed Fan Study. II - Data and Performance - Unslotted Blades and Vanes. Rep. PWA-3653, Pratt & Whitney Aircraft (NASA CR-72667), June 1970.

10. Monsarrat, M. T.; Keenan, M. J.; and Tramm, P. C.: Single-Stage Evaluation of Highly-Loaded High-Mach-Number Compressor Stages. Rep. PWA-3546, Pratt & Whitney Aircraft (NASA CR-72562), July 16, 1969.

11. Jones, B. A.; Oscarson, R. P.; and Clark, C. E.: Single Stage Experimental Evaluation of Variable Geometry Guide Vanes and Stator Blading. Part 5: Overall Performance for Variable Camber Guide Vane and Stator B with Radial and Circumferential Inlet Flow Distortion. Rep. PWA-FR-2640, Pratt & Whitney Aircraft (NASA CR-54558), Dec. 31, 1968.

12. Bailey, Everett E.; and Ruggeri, Robert S.: Experimental Data for Two 1400-Feet-Per-Second Tip Speed Compressor Rotors Operated with Inlet Flow Distortions. NASA TM X-1798, 1969.

13. Koch, C. C.: Experimental Evaluation of Outer Case Blowing or Bleeding of Single Stage Axial Flow Compressor. Part VI - Final Report. Rep. R69AEG256, General Electric Co. (NASA CR-54592), Jan. 30, 1970.

14. Hare, Arthur; and Malley, Harry H.: Cooling Modern Aero Engine Turbine Blades and Vanes. Paper 660053, SAE, Jan. 1966.

15. Esgar, Jack B.: Turbine Cooling. J. Eng. Power, vol. 81, no. 3, July 1959, pp. 226-233.

16. Goldstein, R. J.; Eckert, E. R. G.; and Ramsey, J. W.: Film Cooling with Injection Through a Circular Hole. Rep. HTL-TR-82, Minnesota Univ. (NASA CR-54604), May 14, 1968.

17. Goldstein, R. J.; Eckert, E. R. G.; Eriksen, V. L.; and Ramsey, J. W.: Film Cooling Following Injection Through Inclined Circular Tube. Rep. HTL-TR-91, Minnesota Univ. (NASA CR-72612), Nov. 1969.

18. Spalding, D. B.: A Standard Formulation of the Steady Convective Mass Transfer Problem. Int. J. Heat Mass Transfer, vol. 1, no. 2/3, 1960, pp. 192-207.

19. Gauntner, James W.; Livingood, John N. B.; and Hrycak, Peter: Survey of Literature on Flow Characteristics of a Single Turbulent Jet Impinging on a Flat Plate. NASA TN D-5652, 1970.

20. Hrycak, Peter; Lee, David T.; Gauntner, James W.; and Livingood, John N. B.: Experimental Flow Characteristics of a Single Turbulent Jet Impinging on a Flat Plate. NASA TN D-5690, 1970.

21. Whitney, Warren J.; Szanca, Edward M.; and Behning, Frank P.: Cold Air Investigation of a Turbine with Stator-Blade Trailing-Edge Coolant Ejection. I - Overall Stator Performance. NASA TM X-1901, 1969.

22. Prust, Herman W., Jr.; Behning, Frank P.; and Bider, Bernard: Cold-Air Investigation of a Turbine with Stator-Blade Trailing-Edge Coolant Ejection. II - Detailed Stator Performance. NASA TM X-1963, 1970.

23. Szanca, Edward M.; Schum, Harold J.; and Prust, Herman W., Jr.: Cold-Air Investigation of a Turbine with Stator-Blade Trailing-Edge Coolant Ejection. III - Overall Stage Performance. NASA TM X-1974, 1970.

24. Prust, Herman W., Jr.; Schum, Harold J.; Szanca, Edward M.: Cold-Air Investigation of a Turbine with Transpiration-Cooled Stator Blades. I - Performance of Stator with Discrete Hole Blading. (Proposed NASA Technical Note).

25. Szanca, Edward M.; Schum, Harold J.; Behning, Frank P.: Cold-Air Investigation of a Turbine with Transpiration-Cooled Stator Blades. II - Stage Performance Using Stator with Discrete Hole Blading. (Proposed NASA Technical Note).

26. Stewart, W. L.; and Glassman, A. J.: Advanced Concepts to Increase Turbine Blade Loading. Paper 68-WA/GT-11, ASME, Dec. 1968.

27. Bettner, James L.; and Nosek, Stanley M.: Summary of Tests on Two Highly Loaded Turbine Blade Concepts in Three-Dimensional Cascade Sector. Paper 69-WA/GT-5, ASME, Nov. 1969.

28. Lueders, H. G.; and Roelke, R. J.: Some Experimental Results of Two Concepts Designed to Increase Turbine Blade Loading. Paper 69-WA/GT-1, ASME, Nov. 1969.

29. Armentrout, Everett C.: Development of a High-Frequency-Response Pressure-Sensing Rake for Turbofan Engine Tests. NASA TM X-1959, 1970.

30. Braithwaite, Willis M.; and Vollmar, William R.: Performance and Stall Limits of a YTF30-P-1 Turbofan Engine with Uniform Inlet Flow. NASA TM X-1803, 1969.

31. Meyer, Carl L.; McAulay, John E.; and Biesiadny, Thomas J.: Technique for Inducing Controlled Steady-State and Dynamic Inlet Pressure Disturbances for Jet Engine Tests. NASA TM X-1946, 1970.

32. Braithwaite, Willis M.; Dicus, John H.; and Moss, John E., Jr.: Evaluation with a Turbofan Engine of Air Jets as a Steady-State Inlet Flow Distortion Device. NASA TM X-1955, 1970.

33. Kimzey, W. F.: An Investigation of the Effects of Shock-Induced Turbulent Inflow on a YJ93-GE-3 Turbojet Engine. ARO, Inc. (AEDC-TR-66-198, DDC No. AD-377312 L) Nov. 1966.

34. Povolny, John H.: Stall and Distortion Investigation of a YTF30-P-1 Turbofan Engine. Presented at Air Force Aero Propulsion Lab. Airframe-Propulsion Compatibility Symposium, Miami Beach, Fla., June 24-26, 1969.

35. Coltrin, Robert E.; and Choby, David A.: Steady-State Interactions From Mach 1.98 to 2.58 Between a Turbojet Engine and an Axisymmetric Inlet With 60-Percent Internal Area Contraction. NASA TM X-1780, 1969.

36. Coltrin, Robert E.; and Calogeras, James E.: Supersonic Wind Tunnel Investigation of Inlet-Engine Compatibility. Paper 69-487, AIAA, June 1969.

37. Wasserbauer, Joseph F.: Dynamic Response of a Mach 2.5 Axisymmetric Inlet With Engine or Cold Pipe and Utilizing 60 Percent Supersonic Internal Area Contraction. NASA TN D-5338, 1969.

38. Calogeras, James E.: Experimental Investigation of Dynamic Distortion in a Mach 2.50 Inlet With 60 Percent Internal Contraction and Its Effect on Turbojet Stall Margin. NASA TM X-1842, 1969.

39. Crosby, Michael J.; Neiner, George H.; and Cole, Gary L.: Restart and High Response Terminal Shock Control for an Axisymmetric Mixed-Compression Inlet With 60-Percent Internal Contraction. NASA TM X-1792, 1969.

40. Wilcox, Fred A.; Samanich, Nick E.; and Blaha, Bernard J.: Flight and Wind Tunnel Investigation of Installation Effects on Supersonic Cruise Exhaust Nozzles at Transonic Speeds. Paper 69-427, AIAA, June 1969.

41. Crabs, Clifford C.; Mikkelson, Daniel C.; and Boyer, Earle O.: An Inflight Investigation of Airframe Effects on Propulsion System Performance at Transonic Speeds. Presented at the 13th Annual Symposium of the Society of Experimental Test Pilots, Los Angeles, Calif., Sept. 25-27, 1969.

42. Samanich, Nick E.; and Huntley, Sidney C.: Thrust and Pumping Characteristics of Cylindrical Ejectors Using Afterburning Turbojet Gas Generator. NASA TM X-52565, 1969.

43. Harrington, Douglas E.: Jet Effects on Boattail Pressure Drag of Isolated Ejector Nozzles at Mach Numbers From 0.60 to 1.47. NASA TM X-1785, 1969.

44. Burley, Richard R.; and Mansour, Ali H.: Static Performance of an Auxiliary Inlet Ejector Nozzle Using an Afterburning Turbojet Gas Generator. NASA TM X-1999, 1970.

45. Huntley, Sidney C.; and Samanich, Nick E.: Performance of a 10^{o} Conical Plug Nozzle Using a Turbojet Gas Generator. NASA TM X-52570, 1969.

E-5685

NASA-Lewis-Com'l